

**PHILOSOPHICAL TRANSACTIONS
OF THE ROYAL SOCIETY A**

MATHEMATICAL, PHYSICAL AND ENGINEERING SCIENCES

**Magma chambers vs mush zones: constraining the
architecture of sub-volcanic plumbing systems from
microstructural analysis of crystalline enclaves**

Journal:	<i>Philosophical Transactions A</i>
Manuscript ID	RSTA-2018-0006.R1
Article Type:	Research
Date Submitted by the Author:	n/a
Complete List of Authors:	Holness, Marian; University of Cambridge, Earth Sciences Stock, Michael; University of Cambridge, Earth Sciences Geist, Dennis; Colgate University, Geology
Issue Code (this should have already been entered but please contact the Editorial Office if it is not present):	TM1117
Subject:	Petrology < EARTH SCIENCES, Volcanology < EARTH SCIENCES
Keywords:	enclave, magma chamber, microstructure, crystal mush

SCHOLARONE™
Manuscripts



1
2
3
4
5
6
7
8
9
10
11
12
13
14
15
16
17
18
19
20
21
22
23
24
25
26
27
28
29
30
31
32
33
34
35
36
37
38
39
40
41
42
43
44
45
46
47
48
49
50
51
52
53
54
55
56
57
58
59
60

Magma chambers vs mush zones: constraining the architecture of sub-volcanic plumbing systems from microstructural analysis of crystalline enclaves

Marian B. Holness¹, Michael J. Stock¹, Dennis Geist^{2,3}

1. Department of Earth Sciences, University of Cambridge, Downing Street, Cambridge CB2 3EQ UK.

2. U.S. National Science Foundation, 2415 Eisenhower Ave., Alexandria, VA 22314, USA

3. Geology Department, Colgate University, Hamilton, NY 13346, USA

September 2018

Abstract

There are clear microstructural differences between mafic plutonic rocks that formed in a dynamic liquid-rich environment, in which crystals can be moved and re-arranged by magmatic currents, and those in which crystal nucleation and growth are essentially *in situ* and static. Crystalline enclaves, derived from deep crustal mushy zones and erupted in many volcanic settings, afford a unique opportunity to use the understanding of microstructural development, established from the study of intrusive plutons, to place constraints on the architecture of sub-volcanic systems. Here, we review the relevant microstructural literature, before applying these techniques to interrogate the crystallisation environments of enclaves from the Kameni Islands of Santorini, and Rábida Volcano in the Galápagos. Crystals in samples of deep-sourced material from both case studies preserve evidence of at least some time spent in a liquid-rich environment. The Kameni enclaves appear to record an early stage of crystallisation during which crystals were free to move, with the bulk of crystallisation occurring in a static, mushy environment. In contrast, the Rábida enclaves were sourced from an environment in which hydrodynamic sorting and re-arrangement by magmatic currents were common, consistent with a liquid-rich magma chamber. While presently-active volcanoes are thought to be underlain by extensive regions rich in crystal mush, these examples preserve robust evidence for the presence of liquid-rich magma chambers in the geological record.

Keywords: Magma chamber, enclave, microstructure, crystal mush

Introduction

Over the last few decades, the petrological community has moved away from the idea of sub-volcanic magma being stored in large liquid-rich regions (i.e. magma chambers) towards a model of sub-volcanic plumbing systems that are dominated by hot zones comprising relatively liquid-poor crystal mushes¹⁻³. This paradigm shift, largely based on the absence of geophysical evidence for the presence of large bodies of essentially crystal-free liquid underlying currently active volcanoes, raises many fundamental questions. Although there appear to be no large vats of largely liquid magma currently stored in the crust³, the convincing evidence preserved in the geological record shows that they have existed at other times in Earth history⁴. Furthermore, the geological record preserves evidence of eruption of large volumes of crystal-poor liquid⁵. What governs whether magma occupies big chambers or forms crystal mushy zones? How can large volumes of crystal-poor liquid be assembled if the liquid spends time stored in a crystal-rich mushy zone? Answers to these questions require us to identify such crystal mushy zones in the geological record and to understand how their physical properties (such as rheology and permeability) evolve with time.

In this contribution, we review the evidence preserved in fully solidified intrusions that can be used to distinguish between crystallisation in liquid-dominated and solid-dominated systems, showing how outcrop-scale features relate to the associated rock microstructure. We then discuss how to decode the solidification history of small, out-of-context, fragments of disrupted plutonic material entrained in erupted magmas, using their microstructures alone to deduce the crystallisation regime active during the lifetime of their deep crustal source. We address the problem via a consideration of microstructural features that can only be formed in systems in which crystals can be re-distributed by magmatic currents (i.e. a system containing a large volume of crystal-poor liquid), and those that indicate *in situ* crystal nucleation and growth (i.e. in a less dynamic system more applicable to a mushy zone). We focus on mafic systems, in which the liquid is relatively low viscosity. Finally, we present two case studies of deep crustal fragments erupted by volcanoes in two distinct tectonic environments – the Galápagos (hot spot setting) and Santorini (arc setting).

The petrological signature of a magma chamber

Although there is no evidence to support the existence of such bodies today, it is straightforward to distinguish the endmember magmatic behaviour represented by bodies which formed by the progressive inwards solidification of an essentially crystal-free liquid by examining ancient, fully solidified plutons now exposed at the surface. Inwards solidification is generally manifest in large mafic bodies by a consistent (although often interrupted or repeated) inwards progression from relatively primitive to more evolved compositions⁶. Importantly, such a progression points to efficient fractionation, which is only possible in bodies in which solids can be easily separated

1
2 from the remaining liquid: it is therefore best developed in liquid-rich bodies of low viscosity
3 magma. The Skaergaard Intrusion of East Greenland epitomises such behaviour, having
4 crystallised from a large body of crystal-rich magma that was undisturbed by subsequent
5 replenishment after initial intrusion^{4,6-7}. It is important to point out, however, that Skaergaard
6 represents an unusually clear example of crystallisation from a liquid-rich magma body: it is not
7 always so straightforward to obtain information on the amount of crystal-free liquid present at
8 each moment during the evolution of the intrusion (i.e. how big the magma chamber was through
9 time).
10
11
12
13

14 In smaller mafic intrusions, such as sills, evidence of fractionation of an initially liquid-rich body
15 may be provided by accumulations of dense cargo crystals (pre-existing crystals transported into
16 the reservoir by a carrier melt) on the floor. It has recently been shown that stratigraphic changes
17 in grain size within such accumulations record information about the strength of convection in the
18 magma⁸.
19
20
21

22 On a smaller scale than that of an entire intrusion, fractionation is recorded by compositional
23 zonation towards more evolved compositions on grain margins. Recently, it has been shown that
24 these zoned margins may include a region of constant composition, as a consequence of step-
25 wise thermal buffering along a liquid line of descent in a fractionating system caused by the
26 release of latent heat of crystallisation⁹ (Fig. 1b). Step-wise changes of the composition of the
27 constant composition zone are present in the stratigraphy of large liquid-dominated bodies such
28 as Skaergaard⁹⁻¹⁰. The sequential arrival of new liquid phases as the remaining bulk magma
29 migrates along the liquid line of descent is also recorded in the stratigraphy of fractionating mafic
30 intrusions by step-wise changes in the augite-plagioclase-plagioclase dihedral angle¹¹.
31 Importantly, these methods of detecting the wholesale fractionation of large liquid-dominated
32 bodies require spatial context (i.e. a known position in the intrusion).
33
34
35
36
37

38 The observation of settled blocks with associated disruption of the underlying and surrounding
39 layering¹²⁻¹³ clearly demonstrates not only the presence of a well-defined floor to a magma
40 chamber, but also that the layering itself must have formed directly at an interface between liquid
41 and mush¹². Similarly, evidence of scouring and re-deposition of crystals to form modally-graded
42 layers¹³⁻¹⁵ attests to the actions of magmatic currents on a crystal mush forming on the floor of a
43 crystal-poor magma chamber.
44
45
46

47 Fabrics defined by a shape preferred orientation, defining either a lineation or foliation, form in a
48 liquid-rich environment either during settling or by re-arrangement at the interface between the
49 mush and the overlying magma¹⁶. A fabric created during crystal accumulation in a liquid-rich
50 environment is indicated by the juxtaposition of undeformed euhedral grains (i.e. bounded by
51 growth faces) cemented by anhedral interstitial material (Fig. 1a)¹⁴. Fabrics and microstructures
52 indicative of grain accumulation on the floor of a liquid-rich chamber are typical of modally-
53 graded layers in plutons ranging from gabbros¹²⁻¹⁴ to granodiorite¹⁶. Fabrics may also form in a
54 crystal-rich environment, by shear caused by wholesale pre-consolidation slumping¹⁷⁻²¹ or during
55
56
57
58
59
60

1
2 grain-supported flow during pluton-scale events²²: these are typically not associated with modal
3 layering.
4
5
6

7 **How can we study crystal mushy zones?**

8
9 The abundant and convincing evidence described above supports the existence of melt-rich
10 magma chambers in the plutonic record and has shaped our thinking for decades about what is
11 happening in the magmatic plumbing systems of currently active volcanoes. The new ideas
12 suggesting that magma chambers are not present under currently-active volcanoes³, means that
13 we should not rely on models based on this type of magma storage zone but need instead to find
14 another way of interrogating the deep crust in volcanic regions. One direct source of information
15 is provided by entrained fragments of incompletely solidified cognate mush, derived from depth
16 in the magma source region and found in erupted magmas. These have a range of names in the
17 literature, including cognate xenoliths, or nodules: here we will refer to them as glassy crystalline
18 enclaves, or simply enclaves. These entrained fragments of deep mush are relatively common in
19 the eruptive products of currently active or recent volcanoes²³⁻³¹ and can inform us about the
20 magmatic plumbing system in the present day. Fully solidified (i.e. non-glassy) non-erupted
21 examples of entrained deep-sourced plutonic material may also be exposed by erosion in older
22 settings (e.g. xenoliths in the Skaergaard Campsite Dyke^{10,32})
23
24
25
26
27
28
29

30 In contrast to the study of fully solidified plutons, in which spatial information is available at all
31 scales, there is no spatial context for entrained glassy crystalline enclaves: we need therefore to
32 emulate the scientists who decoded rocks brought back from the Moon during the lunar program
33 and rely on information encoded in the enclaves themselves. In the past, geochemistry has been
34 used as the primary tool to determine the genetic relationships between enclave and host, and to
35 place the enclaves in a wider igneous setting³¹. Geochemical techniques for constraining the
36 pressure and temperature of crystallisation are well-known³³ and will not be addressed here.
37 Instead we will focus on microstructure, which is a relative newcomer to the field. Previous work
38 on this subject has investigated melt distribution in glassy crystalline enclaves³⁴, but here we also
39 include a consideration of microstructural proxies for cooling rate and fluid dynamical regime
40 during crystallisation. This review highlights what we currently know about the environment of
41 enclave formation, using case studies to illustrate our current position (which is dominated by
42 work on mafic rocks) and points to where more work is needed to fully decode the enclaves'
43 record of magmatic processes in a robust and quantitative way across the range of magma
44 compositions.
45
46
47
48
49
50
51
52

53 **Are entrained fragments representative of the deep plumbing system?**

54
55 Entrainment and eruption of a representative sample of the deep regions of a magmatic
56 plumbing system is not straightforward. Perhaps the most fundamental issue concerns the
57
58
59
60

1
2 Stokes settling velocity: large, dense, enclaves are less likely to be erupted compared to smaller,
3 buoyant, enclaves, creating a sample population biased towards more silicic material. Such a
4 bias may be evident in the population of xenoliths entrained in the Campsite Dyke in the
5 Skaergaard intrusion^{10,32}, in which the largest enclaves are plagioclase-rich, while the more mafic
6 examples tend to be the smallest (M.B. Holness, unpublished data). However, in relatively
7 volatile-rich systems enclave bulk density may be reduced by significant gas exsolution which, if
8 it is not sufficient to disintegrate the enclave (see discussion below), may promote ascent³⁵.

9
10
11
12 Entrainment involves the mechanical process of fracturing and dislodging material from its
13 source and this is poorly understood. Of particular relevance is the possibility that the ease of
14 entrainment varies with the geometry, size and orientation of the interface between the
15 ascending magma and the material to be entrained. For example, it is possible that entrainment
16 is easier at vertical surfaces such as conduit walls, compared to the floor of a magma chamber.
17 Although the predominantly laminar flow in narrow dyke-like conduits³⁶ is perhaps ineffective in
18 causing entrainment of sidewall material, entrainment might be more efficient if subsequent
19 injections of magma resulted in re-opening (by brittle failure) of an older conduit.

20
21
22
23
24 Various lines of evidence have been used to infer that enclaves were derived from the chilled
25 side-wall of their source magma body, such as: differences in the primocryst assemblages
26 between the enclaves and host magma²⁵; a higher concentration of enclaves in the earlier parts
27 of the eruption²⁵; the presence of intrusive contacts between mush and country rock within
28 enclaves²⁸; microstructures characterised by loose, high-porosity, frameworks that can be
29 attributed to inwards growth in vertical solidification fronts^{25,28}; and a fine grain-size and low glass
30 content relative to that in the enclave population as a whole²⁹. Although the presence of contacts
31 within the enclave certainly provides incontrovertible evidence that it did indeed derive from the
32 margin of the source body, the other criteria were devised in the context of a paradigm in which
33 eruptions are fed by magma chambers in which solidification occurred on their (vertical) walls
34 while crystals accumulated on a (horizontal) floor. They should be re-visited in the light of our
35 new conception of mushy sub-volcanic magma storage regions.

36
37
38
39
40
41
42 Survival of entrained material during ascent necessitates minimal disaggregation: the survival of
43 crystal-rich fragments therefore depends on their ability to withstand the shearing forces imposed
44 by the magma and the tensile forces due to vesicle expansion. The latter is due not only to
45 reduced solubility of H₂O and CO₂ with decreasing pressure, but also due to the expansion of
46 gas during ascent. These effects become highly significant at pressures lower than a few
47 hundred MPa³⁷, even for relatively H₂O-poor liquids. Since rocks, especially those that are
48 incompletely solidified, have low tensile strengths, enclaves will disintegrate during ascent unless
49 this expansion can be accommodated by loss of either gas or interstitial melt (e.g. gas filter-
50 pressing³⁸). The first relies on the formation of interconnected bubble chains, which occurs above
51 ~ 30 vol% gas³⁹. The second relies on the enclave containing sufficient interstitial melt to
52
53
54
55
56
57
58
59
60

1
2 accommodate vesicle expansion by melt expulsion – this results in the development of glass-rich
3 rinds on enclaves⁴⁰.

4
5 This bias in enclave survival is the most likely reason behind the observation that enclaves
6 generally have >60 vol.% crystals, reflecting the minimum volume fraction of crystals at which a
7 framework of randomly oriented prismatic grains (the dominant texture of high-porosity nodules)
8 retains its integrity during ascent. The bulk volumetric proportion of vesicles in enclaves is
9 generally less than 30 vol.%^{29,35,41}, either due to the strength reduction of the high-porosity
10 enclaves at higher vesicle contents or because this represents the percolation threshold above
11 which vesicles form an interconnected network permitting escape of the excess gas volume³⁹.

12
13 The population of erupted enclaves may therefore not be representative of the crystal mush at
14 depth. The population will be biased towards regions of the mush which are most easily broken
15 to form discrete fragments, with a further bias introduced during ascent: those enclaves which
16 easily disintegrate contribute to the phenocryst load (as xenocrysts or antecrysts) rather than
17 erupting as discrete entities.
18
19

20 21 22 23 24 25 **Microstructural proxies for cooling and crystallisation rates**

26 To determine the source of an enclave we need to differentiate between enclaves derived from
27 the conduit along which the magma travelled and those entrained from the larger magma body
28 feeding the conduit. Conduits are likely to be relatively rapidly cooled due to their limited lateral
29 extent. Consequently, if the enclaves preserve evidence of slow cooling and crystallisation they
30 are more likely to come from a larger body. Enclaves are typically <1-10cm in scale, with rare
31 larger examples provided by the Skaergaard Campsite Dyke xenoliths. Indicators of cooling and
32 crystallisation rates therefore need to be applicable to such small samples. A commonly used
33 geochemical method to constrain cooling rate of such small samples depends on analysis of
34 diffusional modification of step-changes in mineral composition⁴²: here we describe alternative
35 methods based on microstructure.
36
37
38
39
40
41
42

43 *Retention of high-temperature crystallographic structures*

44 Some minerals, such as low-Ca pyroxene and quartz, undergo reconstructive phase transitions
45 during cooling. If cooling happens too quickly for the phase transition, then the high-temperature
46 form is retained at low temperatures. An example of this is observed in cognate gabbroic
47 xenoliths in the Skaergaard Campsite Dyke. This dyke intruded the upper levels of the
48 Skaergaard cumulate stratigraphy while the intrusion was still hot, entraining material from
49 deeper levels in the intrusion. Although all pigeonite in the cumulate stratigraphy of the
50 Skaergaard intrusion is fully inverted to orthopyroxene, those pigeonite primocrysts in the
51 gabbroic xenoliths entrained in the dyke are only partially inverted¹⁰, demonstrating that they
52
53
54
55
56
57
58
59
60

1
2 were relatively rapidly cooled, preventing completion of the reconstructive phase transition from
3 the monoclinic to the orthorhombic structure.
4

5 6 7 *Plagioclase grain shape*

8
9 Plagioclase is an especially informative mineral for reconstructing magmatic processes: it is the
10 most abundant mineral in the Earth's crust; the slow diffusion rates of the major components
11 preserve compositional zoning, and record episodes of growth and dissolution; its generally
12 tabular shape results in shape-preferred orientations that provide information about magmatic
13 flow¹⁴⁻¹⁵; and the shape itself can be used to decode crystallisation timescales.
14
15

16
17 The shape of plagioclase grains growing from a liquid is dependent on the extent of departure
18 from equilibrium, which is in turn dependent on the extent of undercooling⁴³. At large
19 undercoolings, diffusion-limited growth results in swallowtail and spherulitic forms, whereas
20 faceted euhedral grains form at low undercoolings when growth is interface-controlled. The
21 shape of euhedral plagioclase grown at low undercoolings, quantified by the average apparent
22 aspect ratio as observed in thin section, is a systematic function of crystallisation time⁴⁴. The
23 average apparent aspect ratio, AR, shows a well-defined negative correlation with time taken to
24 crystallise. Hence, we can use AR to determine the *minimum* size of the body from which any
25 enclaves were derived.
26
27
28
29
30

31 32 *Grain junction geometry*

33 34 1. Melt-solid-solid junctions

35
36 The shapes of grains, and the geometry of intervening melt-filled pores, in solidifying materials
37 are generally determined by the kinetics of crystal growth. At the crystallisation rates experienced
38 in plutonic environments, growth is interface-controlled, and most minerals of geological
39 relevance grow with planar faces: the geometry of melt-filled pores is therefore governed by the
40 impingement of these planar-sided grains (Fig. 2a). Such a microstructure has a high total
41 interfacial free energy in comparison to texturally equilibrated microstructures which are
42 characterised by smooth curvature of melt-solid interfaces and the establishment of the
43 equilibrium melt-solid-solid dihedral angle at pore corners (Figs. 2b, c). The driving force for
44 textural equilibration is the reduction of interfacial energies, which is generally much smaller than
45 the driving force for chemical equilibration (i.e. crystallisation). Therefore, solidifying systems only
46 approach textural equilibrium if the rate of crystallisation is slow or reduced to zero⁴⁵.
47
48
49
50

51
52 Textural equilibration is achieved first at pore corners, by rotation of large areas of the melt-solid
53 interfaces to create the equilibrium dihedral angle: the corresponding curvature of the interfaces
54 then propagates outwards from the two-grain junctions⁴⁶. The rate at which this equilibration
55 process occurs is not well known: although experiments suggest that equilibrium can be
56
57
58
59
60

1
2 achieved in olivine-basalt aggregates with a grain size of order 0.1mm within a week⁴⁵, grain
3 growth in these experimental charges obscures the timescales of establishment of constant
4 mean curvature at the interfaces. Establishing the rates at which textural equilibrium is
5 approached in the super-solidus should be a focus for future work.
6
7

8 2. Three-grain junctions 9

10 The median dihedral angle at three-grain junctions involving only a single phase is, by
11 geometrical necessity, 120°. The extent of textural equilibration cannot, therefore, be ascertained
12 simply from the median of the dihedral angle population, but must be assessed from a
13 consideration of the extent to which the grain boundaries have constant mean curvature, and
14 from the standard deviation around the median dihedral angle: for isotropic materials this will be
15 zero, increasing commensurately with increasing crystallographic anisotropy of the mineral⁴⁷. In
16 shallow crustal rocks, single-phase three-grain junctions are commonly close to textural
17 equilibrium, whereas the dihedral angles at junctions involving two phases are generally far from
18 equilibrium (Fig. 2d). This difference in the amount of sub-solidus modification of primary igneous
19 microstructures is because equilibration of multi-phase junctions involves significant mass
20 transport along grain boundaries whereas the overprinting of a primary crystallisation geometry
21 at single-phase junctions requires only the migration of grain boundaries⁴⁶.
22
23

24 The microstructural usefulness of plagioclase is further exemplified by the systematic variation in
25 the median value of the disequilibrium augite-plagioclase-plagioclase dihedral angle with cooling
26 rate in mafic intrusions⁴⁸. Augite-plagioclase-plagioclase dihedral angles vary because of the way
27 crystallisation rate affects the rate at which the different plagioclase faces grow⁴⁹ (which, as we
28 have seen, also controls the final shape of plagioclase grains⁴⁴). Because the anisotropy of
29 plagioclase growth is the primary control on disequilibrium dihedral angles, we would expect any
30 three-grain junction involving two grains of plagioclase and a grain of a second phase to show
31 the same systematic variations with crystallisation timescales, as long as the morphology of the
32 second phase did not also have a strong cooling rate control⁴⁹.
33
34
35
36
37
38
39
40
41
42

43 **Melt distribution in the crystal mush**

44 The distribution of glass in incompletely crystallised (predominantly mafic) enclaves has been
45 investigated by Holness et al. (2007)³⁴. They found that melt is very commonly present as thin
46 films on grain boundaries (Fig. 3a). The films do not have parallel sides and locally contain small
47 mineral grains, demonstrating that they are primary and were not created by decompaction
48 during ascent. Holness et al. (2007) also identified features that they termed “impingement
49 lenses”: these are small cusped pockets of glass on irregular grain boundaries, interpreted to
50 result from the growth of the two bounding grains into the remaining intervening pore space
51 (Figs. 3b, c, d)³⁴. Importantly, Holness et al. (2007) demonstrated that the shape of late-
52 crystallising interstitial phases in fully solidified gabbros is consistent with these late-crystallising
53
54
55
56
57
58
59
60

1
2 phases infilling and pseudomorphing the last remaining pockets of melt, arguing that the glass
3 distribution in the super-solidus enclaves is indeed indicative of that in almost fully solidified
4 gabbros³⁴.
5

6
7 Enclaves that were fully crystallised before entrainment can also sometimes betray where the
8 last melt was, if the host magma that brought them to the surface was sufficiently hot to trigger
9 partial melting. The first parts of the enclave to melt will be those with the lowest melting point
10 and, in a fractionating system, these will be the last drops of the most evolved liquid. Gabbroic
11 enclaves in the Skaergaard Campsite dyke demonstrate that partial melting begins at interstitial
12 pockets filled with late-stage mineral assemblages, with melting extending to the albitic rims of
13 the surrounding plagioclase primocrysts¹⁰.
14
15

16
17 If ascent of the enclaves in the host magma is associated with significant exsolution and
18 expansion of a volatile phase, the component grains of the enclave are likely to be pushed apart
19 or broken. This will result in the creation of parallel-sided, vesicular, melt films on grain
20 boundaries and in fractures: such late-stage features are easily distinguishable from the original,
21 pre-entrapment, geometry of the melt-filled pores at depth.
22
23
24
25

26 27 **Evidence for gravitationally-driven compaction**

28
29 Many authors have suggested that deep-seated crystal mushes collapse by viscous deformation
30 driven by gravitational loading⁵⁰⁻⁵⁶, leading to the formation of adcumulates at depth and the
31 creation of large eruptible volumes of crystal-poor liquid⁵. It is generally assumed that the
32 process of compaction occurs by viscous deformation of a crystal framework, in which the solid
33 grains change shape via processes such as dislocation creep, dissolution-reprecipitation, and
34 melt-assisted grain boundary sliding: this viscous compaction is distinct from what can be termed
35 “mechanical compaction”⁵⁷, which is achieved by the re-arrangement of rigid, non-deforming,
36 particles in the magmatic flow regime⁵⁸. Mechanical compaction necessarily occurs at higher
37 melt contents than viscous compaction, and is likely to be recorded by a strong shape-preferred
38 orientation of grains that preserve no evidence of plastic deformation.
39
40
41
42

43
44 For viscous compaction achieved by dislocation creep, a high free dislocation density forms in
45 response to the stress experienced by the system. Lattice misorientations (shown by undulose
46 extinction and low-angle boundaries) are ubiquitous and (tapering) mechanical twins⁵⁸ are
47 common (Fig. 4a). Extensive plastic deformation by dislocation creep results in a crystallographic
48 preferred orientation, controlled by the slip systems active during deformation, and a shape
49 preferred orientation that is required to accommodate the changes in volume during deformation.
50 Dislocation creep is always accompanied by recrystallization, which annihilates dislocations or
51 recovers them into sub-grains and grain boundaries (Fig. 4b) while the ongoing deformation
52 continually generates new dislocations. Recrystallisation will also remove evidence of any
53 primary magmatic zoning. If the rock is cooled immediately after deformation, preventing static
54
55
56
57
58
59
60

1
2 recrystallization, then the microstructures created during dislocation creep will be preserved.
3
4 However, if the dislocation density in the crystals is sufficiently high and the system remains hot
5 (>500°C for plagioclase) after the cessation of deformation, recrystallization will continue under
6 static conditions, erasing any shape preferred orientation: the microstructure will become
7 granular.
8
9

10 At low stress, the deformation required for viscous compaction occurs by diffusive processes.
11 This is essentially pressure-solution, driven by stress-induced chemical potential gradients
12 whereby rock deforms via the diffusion of matter along grain boundaries, through a liquid phase
13 or through the volume of grains⁵⁹. This process is equivalent to diffusion creep, which is a grain-
14 size sensitive process and is always accompanied by grain boundary sliding⁶⁰. Importantly,
15 viscous deformation by a diffusion mechanism will not always leave a clearly identifiable
16 microstructural record. Typical signatures of diffusion-controlled deformation are the truncation of
17 grains of a known original shape, together with interpenetration of grains and the development of
18 sutured contacts, and compositionally distinct overgrowths on faces oriented so that they are
19 under relatively low stress⁵⁹⁻⁶¹. However, apparently sutured grain boundaries can be created
20 during primary solidification in the absence of deformation (see discussion below). Furthermore,
21 highly irregular grain boundaries created during diffusion-controlled deformation are likely to
22 become smooth during cooling, particularly between two grains of the same phase, driven by the
23 reduction of interfacial energies^{46,62}.
24
25
26
27
28
29

30 Importantly, deformation by diffusive processes results in the partial or complete replacement of
31 compositional zoning formed during the early stages of crystallization. Magmatic zoning is
32 typically parallel to growth faces and strongly zoned mineral grains may contain a core recording
33 their original shape. This provides the opportunity to identify any grain interpenetration by
34 pressure-solution. More generally, viscous compaction resulting in dissolution-reprecipitation will
35 obliterate all grain boundaries defined by growth faces on primocrysts and create discontinuities
36 in the magmatic compositional zoning, associated with a localised loss of planar growth faces,
37 particularly at high pressure points created where grains impinge at a high angle.
38
39
40
41
42
43

44 **Microstructural evidence for crystal accumulation vs. *in situ* growth**

45 Crystallisation regimes fall on a spectrum between an endmember in which solidification occurs
46 on the margins of essentially crystal-free bodies of magma, in the manner certainly operating
47 during solidification of the Skaergaard Intrusion, and another endmember represented by a hot
48 mushy zone dominated by crystals in which any liquid-rich bodies of magma were small or short-
49 lived. Microstructures can be used to distinguish between these two regimes.
50
51
52

53 Large bodies of essentially crystal-free magma, especially those with laterally extensive vertical
54 walls, will generally convect, leading to mobilisation and redistribution of crystals. Although
55 convection in horizontal tabular bodies requires the critical Rayleigh number to be exceeded,
56
57
58
59
60

1
2 cooling of magma at vertical walls will always create a gravitational instability that will drive
3 convection on timescales shorter than that for crystallisation if the liquid is not too viscous. As
4 outlined above, it is straightforward to discern evidence for the large-scale convection indicative
5 of a Skaergaard-style magma chamber from field observations. Although their small size and the
6 absence of any spatial context means that we can't use many of these field-based criteria on
7 entrained crystalline enclaves, we can use the microstructural understanding obtained from study
8 of exposed fully solidified bodies to make inferences about the crystallisation regime in the
9 enclave source.
10
11
12
13

14 With rare exceptions²⁶, enclaves and xenoliths are commonly too small to detect modal or grain-
15 size layering created by crystal re-arrangement in magmatic currents. However, particle re-
16 arrangement in a liquid-rich convecting system commonly results in fabric formation defined by a
17 shape preferred orientation of non-equant grains. Unless subsequently affected by compaction,
18 these grains show no evidence of deformation by either dislocation creep or a dissolution-
19 reprecipitation mechanism. The microstructure in such rocks is characterised by planar growth
20 faces on the mobilised grains, and the juxtaposition of the mobilised grains so that these planar
21 growth faces are in contact, with no evidence for indentation. Further evidence in support of
22 crystal accumulation, and hence crystallisation of a liquid-rich magma body, is provided by a
23 uniform grain size. Although a uniform grain size can be achieved in a closed system if
24 solidification involved a single short burst of nucleation followed by crystal growth⁶³, in an open
25 system in which crystals are mobile a uniform grain size is consistent with hydrodynamical
26 sorting (i.e. crystal re-distribution and accumulation).
27
28
29
30
31
32

33 Grain boundary morphology provides an important discriminant of crystallisation regime, being
34 different in an environment in which grains are free to move relative to each other (i.e. a liquid-
35 rich environment typical of a Skaergaard-style magma chamber) compared to one in which
36 crystals nucleate and grow in proximity (i.e. the situation expected for a liquid-poor crystal mush
37 zone or the walls of a large magma chamber). Grains growing in a liquid-rich environment have a
38 shape indicative of the relative rates of growth in different crystallographic directions, and the
39 symmetry of the crystal lattice. Minerals (such as plagioclase) that grow by birth-and-spread
40 mechanisms are bounded by atomically smooth planar faces, whereas minerals that grow in
41 some crystallographic directions by continuous attachment form grains with some areas of
42 rounded melt-solid interface (e.g. quartz)^{64,65}. Isolated grains suspended in a convecting magma
43 form aggregates by synneusis, and these aggregates are typified by planar grain boundaries that
44 are parallel to the growth faces of both grains (Fig. 3e). This can be clearly discerned if the
45 grains are compositionally zoned^{66,67}. In contrast, grain boundaries formed by the impingement
46 of grains in a crystal-rich environment tend to be highly irregular, at random orientations to
47 growth faces of the constituent minerals (Figs. 3b, f), with small pockets of melt [the impingement
48 lenses of Holness et al. (2007)³⁴] that are commonly pseudomorphed by other minerals during
49 further solidification (Fig. 3d). Although irregular grain boundaries can be indicative of pressure
50
51
52
53
54
55
56
57
58
59
60

1
2 solution^{60,68}, the presence of glass-filled impingement lenses demonstrates the primary growth
3 origin of the irregularities.
4

5 Grain boundary morphology does not always provide unambiguous evidence about how they
6 were formed, however, as shown by Means & Park (1994) who observed changes in grain
7 boundary geometry by boundary migration in crystallising, undeformed, samples of a synthetic
8 analogue⁶⁹. They observed boundaries changing from being euhedral with respect to one grain
9 to euhedral with respect to the other during growth. No explanation was offered for this
10 observation, but similar behaviour in clusters of silicate grains can potentially be detected using
11 compositional zoning to detect successive growth phases. In the absence of firm evidence
12 supporting a changing boundary morphology during growth, an assessment of the relative
13 importance of the two types of grain boundary should reveal the timing and extent to which the
14 enclave grew in a hot mush zone or on the margins of a large liquid-rich magma chamber.
15
16
17
18
19
20
21

22 *Distinguishing the location of crystallisation in a liquid-rich magma body.*

23 Critically, the solidification of a magma chamber may involve the inwards-growth of mushy layers
24 on vertical walls as well as accumulation of material at the (sub-) horizontal floor and roof. The
25 microstructures developed in these three environments will be different: is it possible to find
26 microstructural (or geochemical) criteria by which the growth environments can be distinguished
27 from each other as well as from that in a long-lived crystal mushy zone?
28
29
30

31 The best natural laboratories in which to develop the necessary microstructural criteria are
32 layered intrusions. The Eastern Layered Intrusion of Rum, Inner Hebrides of Scotland, had no
33 vertical walls and was most probably sill-like for much of its life⁷⁰. In contrast, the Skaergaard
34 Intrusion is box-like with walls ~4km high^{7,71}. Crystal mushy layers developed on the walls, floor
35 and roof of the Skaergaard, with solidification involving the inwards-propagation of all three.
36 While the gabbroic cumulates formed on the floor of the Skaergaard Intrusion (the Layered
37 Series) have many features in common with the troctolites and gabbros of the Rum Eastern
38 Layered Intrusion, the microstructures in the rocks from the vertical wall (the Marginal Border
39 Series) are distinctly different.
40
41
42
43
44

45 Fabrics are common in both the magma chamber floor cumulates of the Rum Eastern Layered
46 Intrusion and the Skaergaard Layered Series, and are predominantly defined by a shape
47 preferred orientation of “roughly square” tablets of plagioclase flattened parallel to (010),
48 bounded by planar growth faces^{7,14,72} (e.g. Fig. 1a). In Skaergaard, magmatic foliations together
49 with evidence for shearing (grain tiling, grain imbrication, oblique foliation) led Nicolas (1992) to
50 argue that the fabrics result from grain orientation in currents flowing from the walls onto an
51 already consolidated floor⁵⁷. At high stratigraphic levels, plagioclase forms laths that are elongate
52 along [100]⁷³⁻⁷⁴: these are preferentially oriented to define a lineation in sedimentary features
53
54
55
56
57
58
59
60

1
2 known as trough layers, in which the lineation is parallel to the likely direction of flow of crystal-
3 laden magmas^{7,14,72-75}.

4
5
6 Despite the relative proximity of the intrusion margins, the inner parts of the Skaergaard Marginal
7 Border Series are commonly coarser-grained than equivalent rocks of the Layered Series. All
8 regions of the Marginal Border Series are characterised by a wider range of grain sizes in any
9 one sample compared to stratigraphically equivalent cumulates of the Layered Series (Fig. 5).
10 There is no evidence for any preferred orientation of either crystallographic orientation or grain
11 shape in the Marginal Border Series; neither is there any evidence of intra-grain deformation.
12 The randomly oriented plagioclase grains commonly have irregular and sutured mutual grain
13 boundaries (Fig. 3f). Interstitial material is abundant and normal zoning of individual mineral
14 grains is common (Fig. 5b), indicating significant amounts of interstitial overgrowth from a
15 continuously evolving melt⁹. The evolved rims of constant composition that are a feature of
16 plagioclase grains in the lower parts of the Layered Series are absent in the Marginal Border
17 Series⁹. In contrast to the Layered Series, the Marginal Border Series contains none of the
18 reactive symplectites that have been attributed to differential migration of immiscible interstitial
19 liquids, with the loss of the buoyant Si-rich immiscible conjugate triggering reaction between the
20 remaining dense Fe-rich conjugate and the surrounding primocrysts⁷⁶.

21
22
23 These distinctive characteristics of Marginal Border Series rocks can be attributed to the vertical
24 orientation of the wall. The absence of reactive symplectites is because, at any point in the wall,
25 the rising buoyant Si-rich conjugate is replaced by Si-rich liquid of the same composition from the
26 underlying mush: the Si-rich conjugate can only be lost by lateral flow for which there is no
27 driving force. The absence of constant composition rims on plagioclase grains, together with the
28 relative enrichment in interstitial liquid, point to a strongly orthocumulate status. The absence of
29 preferred grain alignment and wide range of grain sizes is consistent with an absence of particle
30 re-arrangement by magmatic currents (since, on a vertical wall adjacent to crystal-poor liquid,
31 any crystals sufficiently poorly-bound to their neighbours to be re-arranged will simply be
32 removed rather than aligned). The wide range of grain sizes, together with the irregular
33 plagioclase-plagioclase grain boundaries, are also consistent with continuous *in situ*
34 heterogeneous nucleation and growth. We would expect similar features to be present in crystal
35 mushes grown on the walls of vertical conduits: additionally, since narrow conduits are likely to
36 cool quickly, any conduit mushes will be fine-grained.

37
38
39 Roof cumulates are necessarily formed either by *in situ* nucleation and growth, or by
40 accumulation of buoyant minerals and grain clusters. Interstitial liquid that is denser than the
41 underlying liquid will be lost from a permeable roof cumulate, while a buoyant liquid will be
42 retained. Although microstructures of roof cumulates have not been studied in detail, some
43 generalisations can be made about their nature from observation of well-exposed examples in
44 the Skaergaard Intrusion.

1
2 The Skaergaard roof cumulates have a generally more silicic bulk composition than their
3 temporal equivalents on the floor and walls⁷⁷⁻⁷⁸. They contain relatively more plagioclase (which
4 is buoyant in the Skaergaard liquid), and abundant interstitial granophyre (thought to have
5 crystallised from the Si-rich conjugate of an unmixed interstitial liquid⁷⁶). There are none of the
6 ilmenite-rich intergrowths that record the crystallisation of pockets of interstitial Fe-rich liquid,
7 suggesting that this dense immiscible conjugate was lost from the roof. The roof cumulates are
8 generally strongly orthocumulate, with abundant late-stage minerals such as apatite^{77,79}. Fabrics,
9 such as lineations and foliations, are not common, but where present are defined by
10 plagioclase⁷: all other primocryst minerals are denser than the remaining liquid, so re-
11 organisation by magmatic currents sweeps them away from the roof. None of the dense phases
12 show the mono-disperse grain size distributions expected for minerals that underwent
13 hydrodynamic sorting, suggesting they grew *in situ*. There is no evidence of plastic deformation,
14 suggesting that viscous compaction (which can only be driven by the upwards gravitational force
15 associated with plagioclase buoyancy) does not occur.

16
17 Although it might not be straightforward to distinguish enclaves derived from the walls of a liquid-
18 rich magma chamber from those derived from a solid-dominated crystal mushy zone, were an
19 eruption sampling a magma chamber, one would expect the suite of enclaves to include at least
20 some examples with microstructural characteristics of either a floor or a roof accumulation.

21 22 23 24 25 26 27 28 29 30 31 **Analytical methods**

32 QEMSCAN images were obtained for the Rabida enclaves using a Quanta 650 F field emission
33 gun scanning electron microscope (SEM), equipped with two Bruker XFlash 6130 energy
34 dispersive spectrometers (EDS), at the Department of Earth Sciences, University of Cambridge.
35 QEMSCAN images were collected with a 7.5 μm pixel resolution. For further information on the
36 analytical procedure see Holness (2015)⁴⁹. The QEMSCAN images were used to create phase
37 maps and maps of Ca concentration, to enable easy visualisation of compositional zoning in
38 plagioclase.

39 40 41 42 43 44 45 **Case study 1: the Kamani Islands, Santorini**

46 The Kamani Islands comprise dacitic lavas erupted in the centre of the Santorini Volcano
47 caldera, which formed during the Minoan eruption 3600 years ago⁷⁹. The exposed rocks on the
48 Kamani Islands record at least nine subaerial eruptions, the last of which formed a dome in 1950.
49 The pre-1950 lava flows contain a variety of crystal-rich glassy mafic enclaves, the majority of
50 which are andesitic. These are interpreted to be the remnants of a layer of replenishing magma
51 that ponded at the base of a magma chamber, which was disrupted and overturned immediately
52 prior to each eruption⁸⁰. The 1950 lava dome also contains these glass-rich andesitic enclaves,
53 which range in size up to 20 cm in diameter, but is unique in containing a significant number of

1
2 much smaller, almost wholly crystalline, enclaves of cognate troctolitic or gabbroic material
3 (which are present, albeit very rare, in the earlier flows). The following discussion focusses
4 entirely on this latter group of enclaves, which are coarse-grained (grain size up to 1 mm), with a
5 low glass and vesicle content, and with a maximum diameter of 5 cm³⁴. They are sub-rounded to
6 angular and many are often enveloped in less dense, highly vesicular crystal-rich material similar
7 to that of the more common type of andesitic enclaves. They are interpreted as fragments of a
8 deep crustal crystal mush.
9

10
11
12 The gabbroic and troctolitic enclaves from Kameni are dominated by plagioclase, with
13 primocrysts of olivine ± pyroxene. They contain clusters of rounded olivine (± clinopyroxene)
14 grains, characterised by planar grain boundaries parallel to the common growth faces of olivine
15 (Fig. 6a), similar to those found in the Shiant Isles Main sill and ascribed to cluster formation by
16 synneusis of crystals suspended in a convecting magma⁸. The enclaves preserve no evidence
17 for primary igneous shape preferred orientations and the plagioclase is notably equant (Figs. 6b,
18 c, d, e). Although there are too few grains in each of these small enclaves to obtain meaningful
19 values for AR, the clearly low aspect ratios contrast with those of plagioclase erupted as
20 phenocrysts in the host lava or in the associated abundant andesitic enclaves, and are
21 consistent with much slower crystallisation rates for the gabbroic/troctolitic enclaves⁴⁴.
22
23

24
25
26
27 There is localised evidence for melt-solid-solid textural equilibration, particularly at olivine-olivine-
28 melt junctions (Fig. 6f), with some limited evidence at plagioclase-plagioclase junctions (Fig. 6b,
29 c, f), consistent with relatively slow crystallisation rates. Some plagioclase-plagioclase-melt
30 junctions have been modified during or after entrainment, with evidence for late-stage rapid
31 growth resulting in the creation of irregular, but curved, plagioclase-melt interfaces⁸¹ (Figs. 6d, f).
32
33

34
35 Plagioclase has strongly faceted edges where in contact with relatively large melt pools (Figs.
36 6c, d, e, f). Grain boundaries between adjacent plagioclase grains are a mixture of planar
37 boundaries that are parallel to growth faces of one or both of the two grains (e.g. Figs. 6b, e), or
38 are irregular, with no relationship with the crystallographic orientation of the two grains. This
39 irregular type contains impingement lenses (Figs. 6c, d, e). That the irregularities in the grain
40 boundaries formed during solidification itself is shown by the fact that planar facets are present
41 on plagioclase grains adjacent to relatively large pools of melt, but this planar morphology breaks
42 down as the melt film between adjacent grains is narrowed during continuing solidification. The
43 irregular boundaries are therefore a consequence of the infilling of melt-filled space by the
44 progressive growth towards each other of two motionless grains.
45
46
47
48

49
50 What can we deduce about the extent to which melt may have been extracted from the crystal
51 mushy source of these enclaves? They record no evidence for dislocation creep, with no
52 distorted grains or evidence of sub-grains (Fig. 6): there is no evidence of viscous compaction.
53 Any melt extraction must therefore have occurred only by diffusive mechanisms, which primarily
54 involve melt on grain boundaries. The planar grain boundaries in the enclaves do not contain
55 optically resolvable melt films and are unlikely to have played a role in either diffusion-
56
57
58
59

1
2 reprecipitation creep or melt-assisted diffusion creep. In contrast, the irregular nascent
3 boundaries forming between adjacent grains that are growing towards each other do contain
4 melt: their irregular geometry may have provided high-stress contacts for dissolution but there is
5 no optically visible evidence for high dislocation densities at these points. Furthermore, melt-
6 assisted creep during compaction would reduce grain boundary irregularity and one might
7 therefore expect a preferred orientation of straight boundaries, reflecting the stress field during
8 compaction: no evidence for this is present, although the enclaves are perhaps too small for a
9 detailed assessment. In summary, there is no good evidence for melt extraction from the mushy
10 source of these enclaves - future work exploring this question should be focussed on larger
11 specimens of incompletely solidified mush in order to detect any preferential orientation of planar
12 vs irregular grain boundaries.
13
14
15
16
17

18 The microstructural evidence preserved in the Kameni gabbroic and troctolitic enclaves suggests
19 that the crystal mushy zone they came from was built progressively by the accumulation of grain
20 clusters (comprising all three primocryst phases) formed by synneusis. Although synneusis is
21 indicative of a melt-rich environment, once the clusters had accumulated to form a mush, this
22 was not then reworked by magmatic currents or other deformation of the mush pile, perhaps
23 indicative of a small non-convecting magma chamber. The low aspect ratio of the plagioclase
24 indicates a slow cooling rate, but this was still sufficiently fast to prevent the geometry of the
25 remaining plagioclase-bounded melt-filled pores to be controlled by minimisation of interfacial
26 energies: we await a quantitative understanding of textural equilibration rates to place firm
27 constraints on the cooling rate (and hence size) of the magma source region. It is unlikely, on the
28 basis of the evidence presented here, that any melt was extracted from the crystal mush. The
29 small size of the gabbroic and troctolitic enclaves and their comparative rarity, particularly in
30 comparison with the much more abundant andesitic enclaves in the Kameni lavas, suggests that
31 entrainment was not as straightforward as those of the associated highly abundant andesitic
32 enclaves. We suggest that they were probably sourced from a deeper body, with their small size
33 and rarity due to the difficulty in erupting material from levels deeper than the shallow chamber
34 that fed the eruptions.
35
36
37
38
39
40
41
42
43
44

45 **Case study 2: Rábida volcano, Galápagos**

46 Rábida volcano forms one of the smallest major islands in the Galápagos Archipelago. It is
47 constructed of a diverse suite of rocks, ranging from primitive olivine-basaltic lavas through
48 icelandite domes to a rhyodacitic ignimbrite. An arcuate fault on the western part of the island
49 strikes NNW and could be the remnants of a mostly buried caldera⁸². Potassium-argon ages of
50 exposed rocks are all within 1.0 ± 0.1 Ma⁸³.
51
52
53

54 We collected a suite of 11 plagioclase-rich cumulate-textured enclaves from a wave-dissected
55 scoria cone on the north coast of the island. The scoria and ash making up the cone have a
56
57
58
59
60

1
2 distinctive red colouration, probably due to limited interaction with seawater during eruption,
3 intermediate in style between Strombolian and Surtseyan. Most of the enclaves are coated with a
4 rind of quenched scoria, but some are isolated rocks with none of the carrier in direct contact.
5 The enclaves range in size up to ~10 cm in diameter. Some are round cobbles, and others have
6 planar margins consistent with a formation by fracturing of the source.
7
8
9

10 The suite of 11 enclaves is dominated by plagioclase tablets with a generally low average aspect
11 ratio (as viewed in thin section), in the range 1.67 ± 0.8 to 2.59 ± 0.15 . There is a wide range of
12 lithologies, encompassing relatively primitive troctolitic compositions to enclaves containing
13 primocrysts of clinopyroxene, oxides, amphibole and abundant apatite. Where present, olivine
14 forms rounded grains (many are strongly oxidised).
15
16

17 A microstructural progression, based on plagioclase morphology, is suggestive of progressive
18 fractionation. The most primitive enclaves contain an abundance of euhedral plagioclase grains,
19 comprising 60-95 vol.% of the mode. The grain size is commonly mono-disperse in any one
20 enclave, in the range 0.2 – 2mm (Figs. 7a, b), but a few of the finer-grained enclaves contain
21 small numbers of grains that are significantly larger than the rest (Figs. 7c, d, e, 8). The
22 plagioclase grains in most of our sample suite are randomly oriented (Figs. 7a, b, c, d) with few
23 clusters joined by planar boundaries parallel to growth faces. The plagioclase in one enclave is
24 strongly aligned to form a foliation (Figs. 7e, 8). Plagioclase grains within a single enclave show
25 a range of compositional zonation, with some grains apparently unzoned and others with either
26 normal, oscillatory or patchy zoning (Figs. 7d, 8). Subordinate quantities of euhedral grains of
27 clinopyroxene (Fig. 7e), oxides (Fig. 7c, d) or olivine may also be present. Clinopyroxene (Figs.
28 7a, b) and quartz (Fig. 7f) may be interstitial phases, and up to 10 vol.% of these enclaves is
29 occupied by glass or voids.
30
31
32
33
34
35

36 The morphology of the plagioclase margins varies from planar to highly irregular. In enclaves
37 with planar plagioclase margins, the spaces between these euhedral grains are filled with either
38 vesicular glass (Fig. 9a) or interstitial clinopyroxene or quartz (Figs. 7a, b, f, 9b). In enclaves with
39 highly irregular plagioclase margins, grain boundary voids and melt films are abundant. Irregular
40 plagioclase margins fall into two types: One is a jigsaw-fit geometry, where grains can be fit
41 together by closing the voids (Figs. 7f, 9b). This type is associated with intragrain fractures (Fig.
42 7f), which are locally occupied by glass (Figs. 9c, d), and is clearly a consequence of
43 decompaction driven by vesiculation of the interstitial liquid during ascent. The other type is
44 characterised by non-parallel-sided and discontinuous impingement lenses (Figs. 9e, f).
45
46
47
48

49 More evolved enclaves, while still rich in plagioclase (40-50 vol.%), are characterised by an
50 abundance of large primocrysts of clinopyroxene, amphibole, and oxides, with subordinate
51 fayalitic olivine (Fig. 10a). Apatite and zircon are abundant. The proportion of glass varies from a
52 few vol.% to 10 vol.%, and apatite is commonly concentrated in, or adjacent to, pockets of glass
53 (Figs. 10a, b). The four enclaves in this category have no preferred orientation of the elongate
54
55
56
57
58
59
60

1
2 grains. The plagioclase grains locally develop a sieve-like texture where adjacent to melt pools
3 (Fig. 10c), indicative of partial melting during/after incorporation into a hotter entraining magma.
4

5
6 There is no evidence of deformation in any of the enclaves, irrespective of either the extent of
7 solidification or modal composition. The abundance of voids on grain boundaries prevents a
8 detailed assessment of three-grain junction geometry, but the preserved corners of glass-filled
9 pores are consistent with a morphology controlled by crystal growth kinetics rather than by the
10 minimisation of interfacial energies.
11
12

13 Our observations are consistent with growth of essentially isolated crystals in a liquid-rich
14 environment followed by accumulation to form a porous mush in which further solidification
15 occurred on the now motionless grains in the mush pile. The rarity of preferred orientations of
16 non-equant grains suggests that reworking of the accumulated crystals by magmatic currents
17 was rare. However, re-working of low aspect ratio grains is not expected to create a strong fabric
18 and, indeed, the single enclave with high aspect ratio plagioclase does have a shape preferred
19 orientation. The mono-disperse grain size distribution in many of the enclaves is suggestive of
20 significant hydrodynamic sorting, and points therefore to re-working of crystal accumulation by
21 magmatic currents. The absence of much evidence for synneusis is intriguing and suggests that
22 the growing grains (particularly plagioclase) did not encounter other grains before final
23 accumulation. The crystal accumulation underwent no discernible deformation that would have
24 resulted in expulsion of interstitial liquid: there is no evidence of viscous compaction.
25
26
27
28
29

30 The microstructures point to the presence of liquid-rich magma bodies beneath Rábida volcano,
31 in which marginal crystal accumulations formed, either by flotation or settling. The mono-disperse
32 grain size distribution and the frequency of non-touching contacts demonstrates there was no
33 significant heterogeneous nucleation that is an essential component of building a mushy layer on
34 a vertical wall. The marginal crystal accumulation must therefore have formed on the floor or roof
35 of these liquid-rich magma bodies.
36
37
38

39 The wide range of zoning types present in any one enclave is consistent with the accumulation of
40 crystals from a wide range of different sources. The same range of zoning types is present in
41 porphyritic Rábida basalts, suggesting that the assembly of a mixed cargo of crystals from a
42 range of sources is important both during the history of a liquid-filled magma chamber and during
43 transport of magma to the surface. The microstructural evidence for large liquid-rich magma
44 bodies preserved in the enclaves shows that a mixed crystal cargo in erupted magma cannot be
45 taken in isolation as evidence for the development of a large sub-volcanic mushy zone by the
46 amalgamation of multiple sills. Using the correlation of Holness (2014)⁴⁴, the AR of the
47 plagioclase in the Rábida enclaves translates into crystallisation timescales of 130 - 2300 years.
48 Taking these timescales to be the thermal time constant (the time taken for a thermal difference
49 to decay to 1/e of its original value) of the magma body in which the plagioclase crystallised
50 indicates magma bodies of dimensions in the range 100 - 800 m. This is within the range of
51 magma body size estimated on the basis of eruptive history and geochemical variations at Wolf
52
53
54
55
56
57
58
59
60

1
2 and Ecuador Volcanoes, which range from 50 - 800 m thick at Wolf⁸⁴ and 120 m thick at
3 Ecuador⁸⁵. It is also consistent with the geophysical and petrologic syntheses that have led to a
4 model of melt-rich sills hosted in a crustal-scale cumulate mush column^{86,87}.
5
6
7

8 **Conclusions and directions for future work**

9

10 Clear microstructural differences characterize plutonic rocks which formed in a dynamic liquid-
11 rich environment, in which crystals can be moved and re-arranged by magmatic currents, and
12 those in which crystal nucleation and growth are essentially *in situ* and static. Identifying these
13 regimes in the magma plumbing systems beneath volcanoes is essential for determining the
14 existence of magma chambers *senso lato* and testing the spatial and temporal ubiquity of the
15 recent trans-crustal mushy zone paradigm. We have shown that, by applying techniques
16 developed on intrusive rocks, microstructural observations of exhumed crystalline enclaves can
17 act as an effective discriminant.
18
19
20
21

22 Crystals in samples of deep-sourced material from both the Kameni Islands of Santorini, and
23 Rábida Volcano in the Galápagos preserve evidence of genesis in a liquid-rich environment. The
24 Kameni enclaves appear to record an early stage during which crystals were free to move, with
25 the bulk of crystallisation occurring in a static, mushy environment. In contrast, the source of the
26 Rábida enclaves was an environment in which hydrodynamic sorting and re-arrangement by
27 magmatic currents were common, consistent with a liquid-rich magma chamber. None of the
28 enclaves from either volcano preserve evidence of compaction.
29
30
31

32 A point which has not been addressed in this paper, and requires significant further work, is the
33 perhaps semantic question of how big does a magma body need to be before it can be termed a
34 "magma chamber". We have discussed four crystallization environments: the floor of a volume of
35 crystal-poor magma, at which crystals are mobilized and accumulate from elsewhere; the roof of
36 a crystal-poor magma chamber in which some crystal accumulation occurs, together with *in situ*
37 nucleation and growth; the walls of a crystal-poor magma volume, which solidify only via *in situ*
38 crystal nucleation and growth; and mushy zones, in which crystallization is only *in situ*. The
39 relative importance of these three environments not only depends on magma viscosity (and
40 hence composition) but also on the geometry of magma bodies, their size, and the timing and
41 volume of any magma replenishments. How large or undisturbed does a magma body need to
42 be in order to exhibit the various microstructural characteristics discussed in this contribution?
43 For example, what would be the crystallization regime in a small lens of crystal-poor melt hosted
44 in a larger mush zone? Refining the ideas presented here should be the target of future work.
45
46

47 There is much scope for further work on the microstructural evolution of sub-volcanic mush. An
48 important question needing to be addressed concerns the importance of magma viscosity in
49 controlling the fluid dynamical behavior and hence the crystallisation regime of magma bodies.
50 We have concentrated on mafic systems, but the fluid dynamical behaviour of a more viscous
51 silicic system, in which there is generally a smaller density difference between solids and liquid,
52 will be very different. Laminar flow is almost certain to dominate^{88,89}: the well-documented
53 examples of modal layering in silicic bodies⁹⁰, strongly reminiscent of those in the mafic
54 Skaergaard Intrusion, are unlikely to have identical microstructures, reflecting the very different
55 flow regime during their formation.
56
57
58
59
60

1
2 The separation of melt from cumulates remains one of the most outstanding questions in igneous
3 petrology, and there is a near absence of microstructural evidence for compaction in the natural
4 record. Although there is overwhelming evidence that fractionation by the separation of crystals
5 and residual liquid is responsible for the compositional diversity of both cumulates and melts in
6 systems ranging from basaltic to silicic, the mechanism by which differentiated melt is extracted
7 from the mush pile is unknown. Future work should be focused on solving this problem.
8
9

10
11 Quantification of the prevalence of many of the features we have described in this contribution,
12 such as planar vs non-planar grain boundaries, grain boundary orientations relative to
13 crystallographic orientations, and the strength of shape-preferred orientations relative to the
14 shape of the constituent grains, are needed in order to place tighter constraints on the
15 crystallisation regime in which they formed, with a particular focus on the relatively neglected
16 rocks that form on the upper surfaces of magma bodies. What is also currently missing from our
17 toolbox is a reliable quantitative speedometer based on the extent of textural equilibration in both
18 the super- and the sub-solidus. Experimental work should focus on the determination of the rates
19 at which equilibrium dihedral angles can be attained, in order to place constraints on the cooling
20 rate (and hence size) of the deep-crustal magma bodies sampled by enclaves. Similarly, if we
21 had quantitative understanding of the rates at which textural equilibrium can be attained in fully
22 solidified rocks we could “read through” any microstructural overprint on ancient plutonic rocks to
23 decode their solidification history, for example in the exhumed roots of ancient volcanic systems.
24
25

26 Finally, the observations described here demonstrate that there are systematic characteristics of
27 melt distribution in partially solidified silicate rocks. At present, we have little understanding of
28 how variations in permeability and porosity in natural examples affect the response of partially
29 solidified materials to seismic waves or electric and magnetic currents: coupling careful
30 observation of the melt distribution to their geophysical response is key to accurate interpretation
31 of the geophysical signals of deep-seated regions of partial melt.
32
33

34 **Authors' contributions**

35 MBH carried out microstructural investigations and wrote much of the main text, MS carried out
36 QEMSCAN and microstructural analysis, and DG interpreted the Galápagos results in terms of
37 the volcanic history.
38
39

40 **Competing Interests**

41 The authors declare that they have no competing interests.
42
43

44 **Acknowledgements**

45 We acknowledge the Royal Society of London who supported the Hooke meeting. Iris Buisman
46 is thanked for support in obtaining and manipulating the QEMSCAN data and images. We thank
47
48
49
50
51
52

1
2 two anonymous referees for their thoughtful and insightful comments which greatly improved an
3 earlier version of this contribution.
4
5

6
7 **Funding Statement**

8 MBH acknowledges support from the Natural Environment Research Council [grant numbers
9 NE/N009894/1 and NE/M013561/1]. MJS received support from a Charles Darwin and
10 Galápagos Islands Fund Junior Research Fellowship at Christ's College, Cambridge. DG's
11 contribution is based upon work while serving at the National Science Foundation and was
12 funded by NSF grant EAR-1145271.
13
14
15
16
17
18
19
20
21
22
23
24
25
26
27
28
29
30
31
32
33
34
35
36
37
38
39
40
41
42
43
44
45
46
47
48
49
50
51
52
53
54
55
56
57
58
59
60

For Review Only

References

1. Marsh, B. (2004) A magmatic mush column rosetta stone: the McMurdo Dry Valleys of Antarctica. *Eos, Transactions American Geophysical Union*, **85**: 497-502
2. Christopher, T.E., Blundy, J., Cashman, K., Cole, P., Edmonds, M., Smith, P.J., Sparks, R.S.J. & Stinton, A. (2015) Crustal-scale degassing due to magma system destabilization and magma-gas decoupling at Soufrière Hills Volcano, Montserrat. *Geochemistry, Geophysics, Geosystems*, **16**: 2797-2811.
3. Cashman, K.V., Sparks, R.S.J. & Blundy, J.D. (2017) Vertically extensive and unstable magmatic systems: a unified view of igneous processes. *Science*, **355**: eaag3055.
4. McBirney, A.R. & Noyes, R.M. (1979) Crystallization and layering of the Skaergaard intrusion. *J Petrol*, **20**: 487-554.
5. Bachmann, O. & Bergantz, G.W. (2004) On the origin of crystal-poor rhyolites: extracted from batholithic crystal mushes. *J Petrol*, **45**: 1565-1582.
6. Salmonsén, L.P. and Tegner, C. (2013) Crystallisation sequence of the Upper Border Series of the Skaergaard Intrusion: revised subdivision and implications for chamber-scale magma homogeneity. *Contrib Mineral Petrol*, **165**: 1155-1171.
7. Wager, L.R. & Deer, W.A. (1939) Geological investigations in East Greenland. Part III. The petrology of the Skaergaard intrusion, Kangerdlussuaq, East Greenland. *Meddelelser om Grønland*, **105**: 352 pp.
8. Holness, M.B., Farr, R. & Neufeld, J.A. (2017) Crystal settling and convection in the Shiant Isles Main Sill. *Contrib Mineral Petrol*, **172**: 7.
9. Namur, O., Humphreys, M.C.S. and Holness, M.B. Crystallisation of interstitial liquid and latent heat buffering on solidifying gabbros: Skaergaard Intrusion, Greenland. *J Petrol*, **55**: 1389-1427.
10. Holness, M.B., Richardson, C. and Andersen, J.C.Ø. (2013b) The campsite dykes: a window into the early post-solidification history of the Skaergaard intrusion, East Greenland. *Lithos*, **182-183**:134-149.
11. Holness, M.B., Namur, O. and Cawthorn, R.G. (2013a) Disequilibrium dihedral angles in layered intrusions: a microstructural record of fractionation. *J Petrol*, **54**: 2067-2093.
12. Scoates, J.S., Lindsley, D.H. and Frost, B.R. (2010) Magmatic and structural evolution of an anorthositic magma chamber: the Poe Mountain intrusion, Laramie Anorthosite Complex, Wyoming. *Can Mineral*, **48**: 851-885.
13. Irvine, T.N., Andersen, J.C.Ø. and Brooks, C.K. (1998) Included blocks (and blocks within blocks) in the Skaergaard intrusion: geological relations and the origins of rhythmic modally graded layers. *Bull Geol Soc Am*, **110**: 1398-1447.
14. Vukmanovic, Z., Holness, M.B., Monks, K. and Andersen, J.C.Ø. (2018) The Skaergaard trough layering: sedimentation in a convecting magma chamber. *Contrib Mineral Petrol*, **173**: 43. <https://doi.org/10.1007/s00410-018-1466-1>
15. Solgadi, F. & Sawyer, E.W. (2008) Formation of igneous layering in granodiorite by gravity flow: a field, microstructure and geochemical study of the Tuolumne Intrusive Suite at Sawmill Canyon, California. *J Petrol*, **49**: 2009-2042.
16. Grout, F. F. (1918) Internal structures of igneous rocks; their significance and origin; with special reference to the Duluth Gabbro. *J Geol*, **26**: 439-458.

17. Higgins, M. D. (1991) The origin of laminated and massive anorthosite, Sept Iles layered intrusion, Quebec, Canada. *Contrib Mineral Petrol*, **106**: 340-354.
18. Meurer, W. & Boudreau, A. (1998) Compaction of igneous cumulates part II: compaction and the development of igneous foliations. *J Geol*, **106**: 293-304.
19. O'Driscoll, B., Hargraves, R., Emeleus, C., Troll, V., Donaldson, C. & Reavy, R. (2007) Magmatic lineations inferred from anisotropy of magnetic susceptibility fabrics in Units 8, 9, and 10 of the Rum Eastern Layered Series, NW Scotland. *Lithos*, **98**: 27-44.
20. O'Driscoll, B., Stevenson, C. T. & Troll, V. R. (2008) Mineral lamination development in layered gabbros of the British Palaeogene Igneous Province: A combined anisotropy of magnetic susceptibility, quantitative textural and mineral chemistry study. *J Petrol*, **49**: 1187-1221.
21. VanTongeren, J.A., Hirth, G. & Kelemen, P.B. (2015) Constraints on the accretion of the gabbroic lower oceanic crust from plagioclase lattice preferred orientation in the Samail ophiolite. *Earth Plan Sci Lett*, **427**: 249-261.
22. Paterson, S. R., Fowler Jr, T. K., Schmidt, K. L., Yoshinobu, A. S., Yuan, E. S. & Miller, R. B. (1998) Interpreting magmatic fabric patterns in plutons. *Lithos*, **44**: 53-82.
23. Wager, L.R. (1962) Igneous cumulates from the 1902 eruption of Soufriere, St. Vincent. *Bulletin Volcanologique*, **24**: 93-99.
24. Becker, H.J. (1977) Pyroxenites and hornblendites from the maar-type volcanoes of the Westeifel, Federal Republic of Germany. *Contrib Mineral Petrol*, **65**: 45-52.
25. de Silva, S.L. (1989) The origin and significance of crystal rich inclusions in pumices from two Chilean ignimbrites. *Geol Mag*, **126**: 159-175.
26. Tait, S.R. (1988) Samples from the crystallising boundary layer of a zoned magma chamber. *Contrib Mineral Petrol*, **100**: 470-483.
27. Tait, S.R., Wörner, G., van den Bogaard, P. & Schminke, H.U. (1989) Cumulate nodules as evidence for convective fractionation in a phonolite magma chamber. *J Volcan Geotherm Res*, **37**: 21-37.
28. Turbeville, B.N. (1993) Sidewall differentiation in an alkali magma chamber: evidence from syenite xenoliths in tuffs of the Latera caldera, Italy. *Geol Mag*, **130**: 453-470.
29. Holness, M.B. & Bunbury, J.M. (2006) Insights into continental rift-related magma chambers: cognate nodules from the Kula Volcanic Province, Western Turkey. *J Volcan Geotherm Res*, **153**: 241-261.
30. Bachmann, O. (2010) The petrologic evolution and pre-eruptive conditions of the rhyolitic Kos Plateau Tuff (Aegean arc). *C Eur J Geosci*, **2**: 270-305.
31. Stock, M.J., Taylor, R.N. & Gernon, T.M. (2012) Triggering of major eruptions recorded by actively forming cumulates. *Scientific Reports*, **2**: 731. doi:10.1038/srep00731
32. Jakobsen, J.K., Tegner, C., Brooks, C.K., Kent, A.J.R., Leshner, C.E., Nielsen, T.F.D. & Wiedenbeck, M. (2010) Parental magma of the Skaergaard intrusion: constraints from melt inclusions in primitive troctolitic blocks and FG-1 dykes. *Contrib Mineral Petrol*, **159**: 61-79.
33. Putirka, K.D. (2008) Thermometers and barometers for volcanic systems. *Rev Mineral Geochem*, **69**: 61-120.
34. Holness, M.B., Anderson, A.T., Martin, V.M., MacLennan, J., Passmore, E. and Schwindinger, K. (2007) Textures in partially solidified crystalline nodules: a window into the pore structure of slowly cooled mafic intrusions. *J Petrol*, **48**: 1243-1264.

- 1
2
3 35. Coombs, M.L., Eichelberger, J.C. & Rutherford, M.J. (2002) Experimental and textural
4 constraints on mafic nodule formation in volcanic rocks. *J Volcan Geotherm Res*, **119**: 125–144.
- 5 36. Delaney, P.T. & Pollard, D.D. (1982) Solidification of basaltic magma during flow in a dyke.
6 *Am J Sci*, **282**: 856–885.
- 7 37. Snyder, D. (2000) Thermal effects of the intrusion of basaltic magma into a more silicic
8 magma chamber and implications for eruption triggering. *Earth Plan Sci Lett*, **175**: 257–273.
- 9 38. Sisson, T.W. & Bacon, C.R. (1999) Gas-driven filter pressing in magmas. *Geology*, **27**: 613–
10 616.
- 11 39. Candela, P.A. (1991) Physics of aqueous phase evolution in plutonic environments. *Am Min*,
12 **76**: 1081–1091.
- 13 40. Bacon, C.R. (1986) Inclusions of mafic magma in intermediate and silicic volcanic rocks. *J*
14 *Geophys Res*, **91**: 6091–6112.
- 15 41. Thomas, N. & Tait, S.R. (1997) The dimensions of magmatic inclusions as a constraint on
16 the physical mechanism of mixing. *J Volcan Geotherm Res*, **75**: 167–178.
- 17 42. Hartley, M.E., Morgan, D.J., MacLennan, J., Edmonds, E. & Thordarson, T. (2016) Tracking
18 timescales of short-term precursors to large basaltic fissure eruptions through Fe-Mg diffusion in
19 olivine. *Earth Plan Sci Lett*, **439**: 58-70.
- 20 43. Lofgren, G. (1974) An experimental study of plagioclase crystal morphology: isothermal
21 crystallization. *Am J Sci*, **274**: 243–273.
- 22 44. Holness, M.B. (2014) The effect of crystallization time on plagioclase grain shape in dolerites.
23 *Contrib Mineral Petrol*, **168**: 1076. DOI 10.1007/s00410-014-1076-5.
- 24 45. Holness, M.B. & Siklos, S.T.C. (2000) The rates and extent of textural equilibration in high-
25 temperature fluid-bearing systems. *Chem Geol*, **162**: 137-153.
- 26 46. Hunter, R.H. (1987) Textural equilibrium in layered igneous rocks. In: Parsons, I. (ed.)
27 *Origins of Igneous Layering*. D. Reidel Publishing Company. pp 473-503.
- 28 47. Kruhl, J.H. (2001) Crystallographic control on the development of foam textures in quartz,
29 plagioclase and analogue material. *Int J Earth Sci*, **90**: 104-117.
- 30 48. Holness, M.B., Richardson, C. & Helz, R.T. (2012a) Disequilibrium dihedral angles in dolerite
31 sills: a new proxy for cooling rate. *Geology*, **40**: 795–798.
- 32 49. Holness, M.B. (2015) Plagioclase growth rates control three-grain junction geometry in
33 dolerites and gabbros. *J Petrol*, **56**: 2117-2144.
- 34 50. Wager, L. R., Brown, G. M. & Wadsworth, W. J. (1960) Types of igneous cumulates. *J Petrol*,
35 **1**: 73-85.
- 36 51. Irvine, T. N. (1980) Magmatic infiltration metasomatism, double diffusive fractional
37 crystallisation and adcumulus growth in the Muskox Intrusion and other layered intrusions. In:
38 Hargraves, R. B. (ed.). *Physics of Magmatic Processes*. Princeton, N.J.: Princeton University
39 Press, 325-383.
- 40 52. Sparks, R. S. J., Kerr, R. C., McKenzie, D. P. & Tait, S. R. (1985) Postcumulus processes in
41 layered intrusions. *Geol Mag*, **122**: 555-568.
- 42 53. Shirley, D. N. (1986) Compaction of igneous cumulates. *J Geol*, **94**: 795-809.
- 43 54. Tharp, T. M., Loucks, R. R. & Sack, R. O. (1998) Modeling compaction of olivine cumulates
44 in the Muskox intrusion. *Am J Sci*, **298**: 758- 790.
- 45
46
47
48
49
50
51
52
53
54
55
56
57
58
59
60

- 1
2
3 55. Tegner, C., Thy, P., Holness, M. B., Jakobsen, J. K. & Leshner, C. E. (2009) Differentiation
4 and Compaction in the Skaergaard Intrusion. *J Petrol*, **50**: 813-840.
- 5 56. McKenzie, D. (2011) Compaction and crystallization in magma chambers: towards a model
6 of the Skaergaard Intrusion. *J Petrol*, **52**: 905-930.
- 7
8 57. Holness, M.B., Vukmanovic, Z. & Mariani, E. (2017) Assessing the role of compaction in the
9 formation of adcumulates: a microstructural perspective. *J Petrol*, **58**: 643-674.
- 10 58. Nicolas, A. (1992) Kinematics in magmatic rocks with special reference to gabbros. *J Petrol*,
11 **33**: 891-915.
- 12
13 59. Rutter, E.H. (1983) Pressure solution in nature, theory and experiment. *J Geol Soc Lon*, **140**:
14 725-740.
- 15
16 60. McClay, K.R. (1977) Pressure solution and Coble creep in rocks and minerals: a review. *J*
17 *Geol Soc Lon*, **134**: 57-70.
- 18
19 61. Cooper, M.R. & Hunter, R.H. (1995) Precision serial lapping, imaging and three-dimensional
20 reconstruction of minus-cement and post-cementation intergranular pore-systems in the Penrith
21 Sandstone of north-western England. *Min Mag*, **59**: 213-220.
- 22
23 62. Hunter, R. H. (1996) Textural development in cumulate rocks. In: Cawthorn, G. A. (ed.)
24 *Layered Intrusions*: Elsevier Science B.V., pp. 77-101.
- 25
26 63. Marsh, B.D. (1988) Crystal size distribution (CSD) in rocks and the kinetics and dynamics of
27 crystallization. I. Theory. *Contrib Mineral Petrol*, **99**: 277-291.
- 28
29 64. Kirkpatrick, R.J. (1975) Crystal growth from the melt: a review. *Am Min*, **60**: 798-814
- 30
31 65. Kirkpatrick, R.J. (1981) Kinetics of crystallization of igneous rocks. *Rev Mineral*, **8**: 321-398
- 32
33 66. Beane, R. & Wiebe, R.A. (2012) Origin of quartz clusters in Vinalhaven granite and porphyry,
34 coastal Maine. *Contrib Mineral Petrol*, **163**: 1069-1082.
- 35
36 67. Graeter, K.A., Beane, R.J., Deering, C.D., Gravley, D. & Bachmann, O. (2015) Formation of
37 rhyolite at the Okataina Volcanic Complex, New Zealand: new insights from analysis of quartz
38 clusters in plutonic lithics. *Am Min*, **100**: 1778-1789.
- 39
40 68. Wassmann S, Stöckhert B (2013) Rheology of the plate interface – dissolution precipitation
41 creep in high pressure metamorphic rocks. *Tectonophysics*, **608**: 1-29.
- 42
43 69. Means, W.D. & Park, Y. (1994) New experimental approach to understanding igneous
44 texture. *Geol*, **22**: 323-326.
- 45
46 70. Emeleus, C.H., Cheadle, M.J., Hunter, R.H., Upton, B.G.J & Wadsworth, W.J. (1996) The
47 Rum layered suite. *Developments in Petrology* **15**: 403-440.
- 48
49 71. Nielsen, T.F.D. (2004) The shape and volume of the Skaergaard intrusion, Greenland:
50 implications for mass balance and bulk composition. *J Petrol*, **45**: 507–530.
- 51
52 72. Brothers, R. (1964) Petrofabric analyses of Rhum and Skaergaard layered rocks. *J Petrol*, **5**:
53 255-274.
- 54
55 73. Gay, P. & Muir, I.D. (1962) Investigation of the feldspars of the Skaergaard intrusion, Eastern
56 Greenland. *J Geol*, **70**: 565-581.
- 57
58 74. Nwe, Y.Y. (1975) Aspects of the mineralogy of the Skaergaard intrusion, East Greenland.
59 *Unpublished PhD thesis, University of Cambridge*.
- 60 75. Irvine, T. (1983) Skaergaard trough-layering structures. *Yearbook of the Carnegie Institute of*
Washington, **82**: 289-295.

- 1
2
3 76. Holness, M. B., Stripp, G., Humphreys, M. C. S., Veksler, I. V., Nielsen, T. F. D. & Tegner, C.
4 (2011) Silicate liquid immiscibility within the crystal mush: Late-stage magmatic microstructures
5 in the Skaergaard intrusion, East Greenland. *J Petrol*, **52**: 175-222.
- 6 77. Naslund, H.R. (1984) Petrology of the Upper Border Series of the Skaergaard Intrusion. *J*
7 *Petrol*, **25**: 185-212.
- 8 78. McBirney, A.R. (1989) The Skaergaard Layered Series: I. Structure and average
9 compositions. *J Petrol*, **30**: 363-397.
- 10 79. Salmonsén, L.P. & Tegner, C. (2013) Crystallisation sequence of the Upper Border Series of
11 the Skaergaard Intrusion: revised subdivision and implications for chamber-scale magma
12 homogeneity. *Contrib Min Petrol*, **165**: 1155-1171
- 13 79. Hammer, C.U., Clausen, H.B., Frierich, W.L., and Tauber, H. (1987) The Minoan eruption of
14 Santorini in Greece dated to 1645 BC? *Nature*, **328**, 517-517.
- 15 80. Martin, V.M., Holness, M.B., and Pyle, D.M. (2006) Textural analysis of magmatic enclaves
16 from the Kameni Islands, Santorini, Greece. *J Volcan Geotherm Res*, **154**: 89-102.
- 17 81. Holness, M.B., Humphreys, M.C.S., Sides, R., Helz, R.T. & Tegner, C. (2012b) Toward an
18 understanding of disequilibrium dihedral angles in mafic rocks. *J Geophys Res*, **117**: B06207,
19 doi:10.1029/2011JB008902
- 20 82. Bercovici, H., Geist, D., Harpp, K.S., Almeida, M., Mahr, J., Pimentel, R. & Cleary, Z. (2016)
21 A little island with a big secret: Isla Rábida, Galápagos. *AGU Fall Meeting Abstracts*, V53C-3117
- 22 83. Swanson, F.J., Baitis, H.W., Lexa, J. & Dymond, J. (1974) Geology of Santiago, Rábida, and
23 Pinzón Islands, Galápagos. *Bull Geol Soc Am*, **85**: 1803-1810.
- 24 84. Geist, D.J., Fornari, D.J., Kurz, M.D., Harpp, K.S., Adam Soule, S., Perfit, M.R. & Koleszar,
25 A.M. (2006) Submarine Fernandina: Magmatism at the leading edge of the Galápagos hot
26 spot. *Geochemistry, Geophysics, Geosystems*, **7**: doi.org/10.1029/2006GC001290.
- 27 85. Geist, D., White, W.M., Albarede, F., Harpp, K., Reynolds, R., Blichert-Toft, J. & Kurz, M.D.
28 (2002) Volcanic evolution in the Galápagos: The dissected shield of Volcan
29 Ecuador. *Geochemistry, Geophysics, Geosystems*, **3**: doi.org/10.1029/2002GC000355.
- 30 86. Geist, D. J., Bergantz, G. & Chadwick, W.W. (2014) Galapagos Magma Chambers, in: The
31 Galapagos: A Natural Laboratory for the Earth Sciences, edited by K. S. Harpp, E. Mittelstaedt,
32 N. d'Ozouville and D. W. Graham, vol. 204, 55 pp., John Wiley & Sons, Inc, Hoboken, N. J.,
33 doi:10.1002/9781118852538.ch5.
- 34 87. Davidge, L., Ebinger, C., Ruiz, M., Tepp, G., Amelung, F., Geist, D., Coté, D. & Anzieta, J.
35 (2017) Seismicity patterns during a period of inflation at Sierra Negra volcano, Galápagos Ocean
36 Island Chain. *Earth Plan Sci Lett*, **462**: 169-179.
- 37 88. Glazner, A.F. (2014) Magmatic life at low Reynolds number. *Geology*, **42**: 935-938.
- 38 89. Clemens, J.D. (2015) Magmatic life at low Reynolds number. *Geology*, **43**: e357.
39 doi:10.1130/G36512C.1
- 40 90. Wiebe, R.A., Jellinek, A.M. & Hodge, K.F. (2017) New insights into the origin of ladder dikes:
41 implications for punctuated growth and crystal accumulation in the Cathedral Peak granodiorite.
42 *Lithos*, **277**: 241-258.
- 43
44
45
46
47
48
49
50
51
52
53
54
55
56
57
58
59
60

Figure Captions

Figure 1 - QEMSCAN maps of Ca distribution in cumulates from the Layered Series of the Skaergaard Intrusion, East Greenland. (a) the leucocratic portion of a modal layer from Trough G in Upper Zone. Plagioclase is teal (with darker colours showing more sodic compositions), interstitial phases are quartz (black) and clinopyroxene (grey). Note the euhedral shape of the plagioclase, with most grain boundaries formed by the juxtaposition of these planar growth faces. Although some boundaries show evidence of indentation, the smoothness of these boundaries and the localized presence of late-stage albite on them, together with the absence of a preferred orientation of the late-stage albitic overgrowths on the plagioclase, demonstrates that these indentations are not a consequence of dissolution-reprecipitation in response to an applied stress but are most likely a consequence of irregular, late-stage growth of grains accumulated on the magma chamber floor. The scale bar is 1mm long. (b) a troctolitic cumulate from Lower Zone. Plagioclase is dark teal, with dark relatively albitic rims. Olivine is grey and augite is bright blue. Low-Ca pyroxene (inverted pigeonite) is a mottled grey. The cores of the plagioclase grains formed close to the magma-mush interface while the constant composition relatively sodic rims formed within the mush. The scale bar is 2 mm long.

Figure 2 – (a) Glass-rich portion of the upper crust of the Kilauea Iki lava lake, quenched during drilling. Plagioclase (labelled plag), augite (labelled cpx) and ilmenite (opaque) form a framework with interstitial brown glass (labelled glass). The junctions between adjacent grains are formed by the meeting of planar growth faces (examples are arrowed) with no evidence for minimization of interfacial energies. Plane polarized light. Scale bar is 1 mm long. (b) Plagioclase-rich glassy enclave from Brandur, Iceland, photographed with sensitive tint plate under crossed polars. The glass-filled pores have rounded cusped margins, with low, equilibrium values of the melt-plagioclase-plagioclase dihedral angle established at pore corners (examples are arrowed). Scale bar is 0.5 mm long. (c) Olivine-rich glassy enclave from Mauna Loa, Hawaii. The rounded olivine grains display dihedral angles close to textural equilibrium at pore corners. Plane polarized light. Scale bar is 0.5 mm long. (d) Troctolitic cumulate from the Eastern Layered Intrusion of the Rum Igneous Complex, Inner Hebrides. Three-grain junctions involving only plagioclase are close to textural equilibrium, with a well-developed granular microstructure in plagioclase-only regions. Note the absence of any evidence of planar plagioclase growth faces, in contrast to Fig. 1a. The olivine grain on the right has a low dihedral angle where it forms a three-grain junction with two plagioclase grains (arrowed), demonstrating an absence of textural equilibration of this poly-phase junction. Crossed polars. Scale bar is 0.5 mm long.

Figure 3 – (a) glassy crystalline enclave from Mauna Loa, Hawaii, with an irregular glass film separating grains of olivine (ol) and augite (cpx). Note the small grain of spinel (labelled ox) sitting in the melt film, demonstrating its primary origin during solidification. Plane polarized light. Scale bar is 0.5 mm long. (b) Plagioclase-rich glassy enclave from Brandur, Iceland, showing lenses of glass (examples are arrowed) on irregular grain boundaries. Crossed polars. Scale bar is 1mm long. (c) glassy crystalline enclave from Mauna Loa, Hawaii, with irregular glass pockets (some of which are labelled gl) on boundaries between olivine and orthopyroxene (labelled opx). Note the low dihedral angles at pore corners, denoting approach to super-solidus textural equilibrium. Crossed polars. Scale bar is 0.5 mm long. (d) Plagioclase-rich enclave from Brandur, Iceland, showing a small pocket of glass on a plagioclase-plagioclase grain boundary, now partially infilled by clinopyroxene. Plane polarized light. Scale bar is 0.5 mm long. (e) The chilled margin of the Bracken Bay-Straiton Dyke, SW Scotland, showing a cluster of plagioclase phenocrysts set in a fine-grained groundmass. Note the alignment of the plagioclase and that they are joined along large areas of planar grain boundary parallel to the growth faces. Crossed polars. Scale bar is 0.5 mm long. (f) Gabbro from the Marginal Border Series of the Skaergaard Intrusion, East Greenland, showing highly irregular grain boundaries between adjacent plagioclase grains. Very few of these grain boundaries are parallel to growth faces of the

1
2 plagioclase. Crossed polars with sensitive tint plate. Scale bar is 1 mm long.
3

4 Figure 4 – Cumulates from Middle Zone of the Rustenburg Layered Series of the Bushveld
5 Complex, South Africa. (a) Note the abundant tapering and curved deformation twins in the
6 plagioclase, and the irregular grain boundaries. Cumulus orthopyroxene grains are also bent
7 although neighbouring interstitial clinopyroxene is not strongly deformed. Crossed polars. Scale
8 bar is 1 mm long. (b) Grain boundaries between strongly deformed, original igneous, plagioclase
9 grains are decorated with undeformed neoblasts that grew as a result of dynamic
10 recrystallization. Crossed polars. Scale bar is 0.5 mm long.
11

12 Figure 5 – Sample 458220 from Lower Zone (LZa) of the Skaergaard Layered Series, in which
13 plagioclase is cumulus and augite in interstitial. Note the small range in plagioclase grain sizes
14 and the wide constant composition relatively albitic rims (examples are marked with an asterisk).
15 This sample has only a very weak fabric. Crossed polars. Scale bar is 1 mm long. (a) Sample
16 from the LZa equivalent in the Marginal Border Series. Note the wide range of grain sizes of the
17 plagioclase and the abundant normal zoning (examples are marked with an asterisk). Crossed
18 polars. Scale bar is 1 mm long.
19

20 Figure 6 – Troctolitic and gabbroic glass-bearing enclaves entrained in the 1950 andesite flow of
21 the Kameni Islands, Santorini. (a) Clusters of euhedral to subhedral olivine and augite grains,
22 joined by large areas of planar grain boundary consistent with a formation during synneusis.
23 Crossed polars. Scale bar is 1 mm long. (b) Plagioclase grains in this enclave have low aspect
24 ratios, commonly with complex twinning, and no evidence for dislocation creep (the yellow
25 birefringence colour is due to the thickness of this thin section). The arrowed grain boundary is
26 planar, melt-free and joins two plagioclase grains on their (010) faces: this is suggestive of
27 sintering following synneusis. The grain marked with an asterisk is joined by similarly straight,
28 (010) parallel grain boundaries to adjacent grains. Crossed polars. Scale bar is 1 mm long. (c)
29 While many plagioclase grains have low aspect ratio, some are more elongate, with evidence of
30 sintering following synneusis (grain marked with an asterisk). Note the planar growth faces
31 where plagioclase is adjacent to large pockets of melt (example is marked by an arrow). Crossed
32 polars. Scale bar is 1 mm long. (d) The grain marked with an asterisk has planar growth facets
33 where it protrudes into a large melt-filled pocket (note the serrated, pale grey margins – these
34 grew rapidly after entrainment). The two arrows show the location of wide melt-filled boundaries
35 bounded by highly irregular plagioclase growth faces. Continued growth of these grains will result
36 in the trapping of residual melt to form impingement lenses. Crossed polars. Scale bar is 1 mm
37 long. (e) The two white arrows on the left denote wide melt films on developing grain boundaries
38 between plagioclase grains, whereas those on the right show the location of highly irregular grain
39 boundaries formed by impingement growth. Crossed polars. Scale bar is 1 mm long. (f) The
40 rounded olivine grains have low dihedral angles where in contact (arrowed) denoting some
41 approach to textural equilibrium at pore corners. There is rather less evidence of textural
42 equilibration at plagioclase-plagioclase junctions, with some rounding caused by diffusion-limited
43 late-stage growth during quenching (an example on the left of the image is arrowed – note the
44 clearly defined smooth inner surface of the overgrowth rim compared with the more irregular
45 outer surface adjacent to the interstitial quenched glass; Holness et al., 2012b). Plane polarised
46 light. Scale bar is 0.5 mm long.
47
48
49

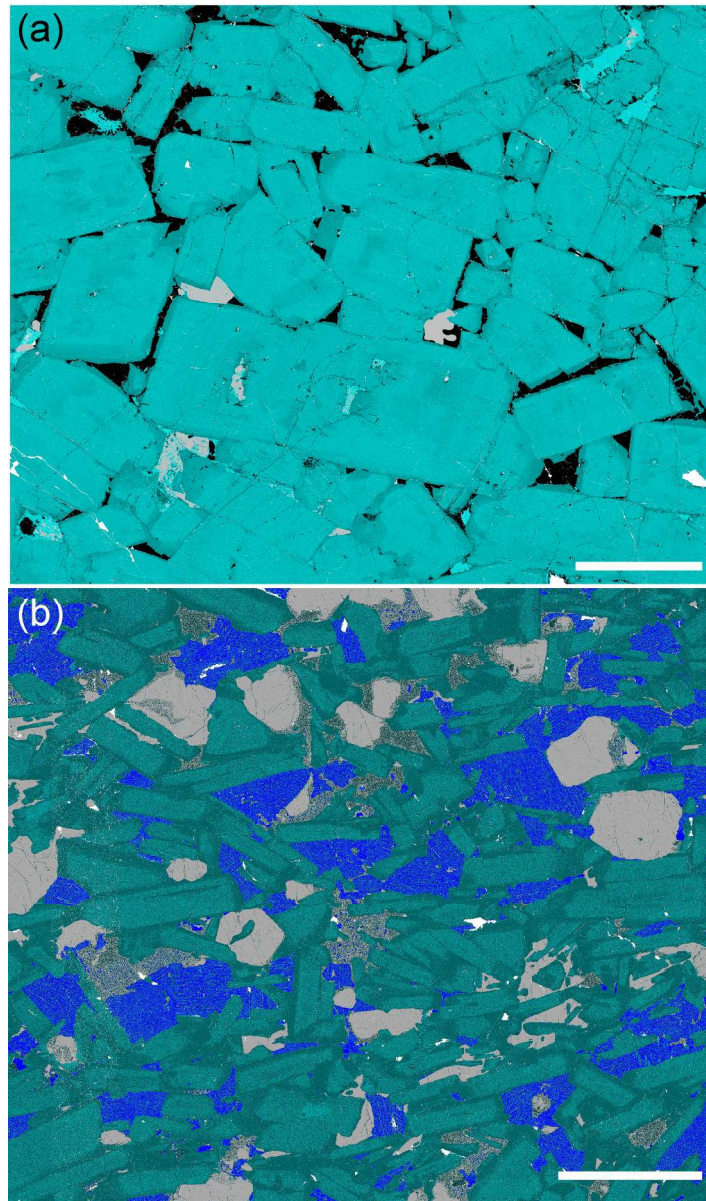
50 Figure 7 – Photomicrographs of the Rábida enclaves, Galápagos. (a) Plagioclase-rich enclave,
51 with interstitial clinopyroxene and vesicular glass, photographed under plane polarised light. (b)
52 shows the same area photographed under crossed polars. Note the absence of preferred
53 orientation of the euhedral, low aspect ratio, plagioclase grains, their uniform grain size, and the
54 frequency with which grain boundaries are formed by the juxtaposition of planar growth faces.
55 Scale bar in both images is 1 mm long. (c) Plagioclase-rich enclave, with abundant small
56 rounded grains of oxide and interstitial vesicular glass, photographed under plane polarised light.
57
58
59
60

1
2
3 (d) shows the same area photographed under crossed polars. The range of grain sizes in this
4 enclave is large, and the larger grains are commonly normally zoned. Note the evidence for
5 complex zoning, with other grains apparently not zoned at all. The scale bar in both images is 1
6 mm long. (e) A strong preferred orientation of relatively elongate plagioclase. Note the scattering
7 of small equant clinopyroxene grains. Crossed polars. Scale bar is 1 mm long. (f) Euhedral,
8 equant plagioclase grains are separated by irregular but parallel-sided voids, with some
9 transgranular fractures. The grain boundary voids are likely to have been created by
10 decompaction caused by devolatilisation of interstitial melt during ascent. Note the interstitial
11 quartz (labelled qtz; examples are arrowed), which is also separated from the adjacent
12 plagioclase by parallel-side voids. Crossed polars. Scale bar is 1 mm long.

13
14 Figure 8 – QEMSCAN images highlighting the Ca content of plagioclase in the Rábida enclaves,
15 Galápagos. Bright colours denote high Ca content and the darker teal more albitic compositions:
16 phases other than plagioclase are black in these images. (a) same enclave as depicted in
17 Figures 7c and d. Note the presence of several different zoning patterns, with particular
18 examples of either normal, patchy or oscillatory zoning marked by asterisks. It is not possible to
19 reproduce this range of apparent zoning types by sectioning through a single type. Scale bar is 2
20 mm long. (b) same enclave as depicted in Figure 7e. The two large plagioclase grains either side
21 of the asterisk are the two larger grains shown in Figure 7e. Note the strong preferred
22 orientation. The relatively larger grains in this field of view have strongly calcic cores, in contrast
23 to the majority of the smaller grains which have complex partially resorbed cores attesting to a
24 different growth history. Scale bar is 2 mm long.

25
26 Figure 9 – Photomicrographs of the Rábida enclaves, Galápagos. (a) Euhedral plagioclase and
27 rounded grains of Fe-Ti oxides, set in highly vesicular interstitial glass. Plane polarised light.
28 Scale bar is 0.5 mm long. (b) All grain boundaries in this enclave have been opened and are now
29 either voids or locally contain some vesicular glass. Note the abundant interstitial quartz.
30 Crossed polars. Scale bar is 1 mm long. (c) A grain boundary containing vesicular glass
31 separates two plagioclase grains, photographed under plane polarised light. The same area is
32 photographed under crossed polars in (d), in which it is apparent that the grain boundary has
33 been opened by decompaction caused by devolatilisation during ascent, as the newly opened
34 fracture also cuts one of the plagioclase grains. Scale bar in both images is 0.5 mm long. (e)
35 Interstitial pockets of vesicular glass are bounded by either planar plagioclase growth faces (with
36 localised limited approach to texturally equilibrated dihedral angles) or form impingement lenses
37 along grain boundaries. Crossed polars with a sensitive tint plate. Scale bar is 0.5 mm long. (f)
38 Irregular grain boundary between two plagioclase grains, containing vesicular glass. Crossed
39 polars with a sensitive tint plate. Scale bar is 0.5 mm long.

40
41
42 Figure 10 - Photomicrographs of the Rábida enclaves, Galápagos. (a) Enclave containing
43 primocrysts of plagioclase, clinopyroxene, Fe-Ti oxides, with abundant apatite. The central part
44 of this image is magnified in (b) Plane polarized light. Scale bar is 1 mm long. (b) Primocrysts of
45 apatite (labelled ap) are concentrated in, or adjacent to, pockets of glass, demonstrating that
46 they crystallised relatively late. Plane polarized light. Scale bar is 0.5 mm long. (c) Plagioclase
47 adjacent to pockets of (oxidized) glass or minerals that arrive relatively late on the liquidus has
48 developed a sieve texture consistent with partial melting of the most evolved (and hence with the
49 lowest temperature of crystallization) regions of the enclave during entrainment and ascent in a
50 relatively hot magma. Plane polarized light. Scale bar is 1 mm long.

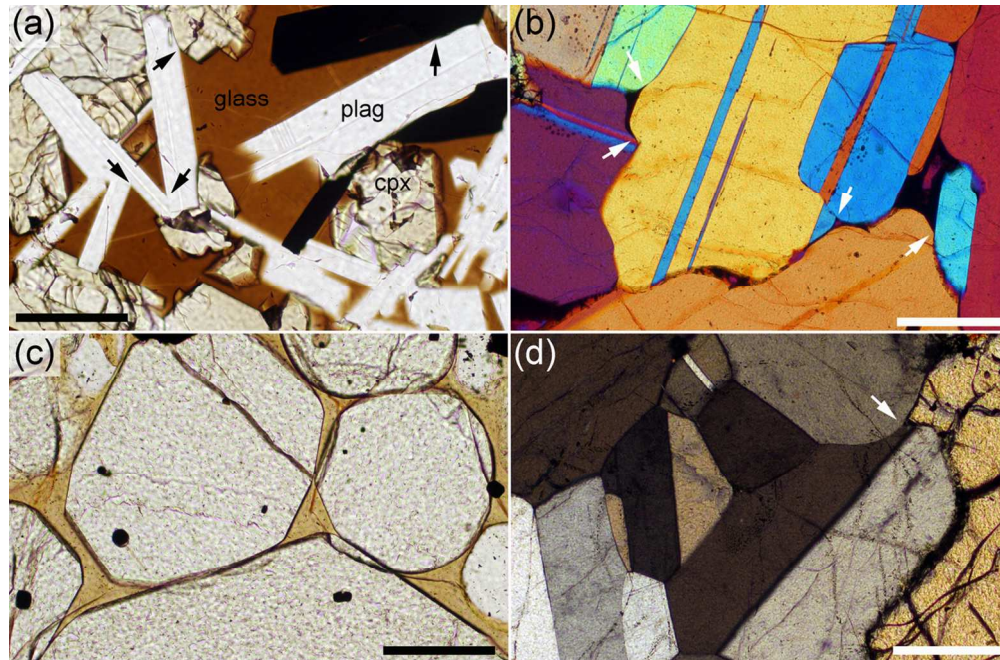


QEMSCAN maps of Ca distribution in cumulates from the Layered Series of the Skaergaard Intrusion, East Greenland. (a) the leucocratic portion of a modal layer from Trough G in Upper Zone. Plagioclase is teal (with darker colours showing more sodic compositions), interstitial phases are quartz (black) and clinopyroxene (grey). Note the euhedral shape of the plagioclase, with most grain boundaries formed by the juxtaposition of these planar growth faces. Although some boundaries show evidence of indentation, the smoothness of these boundaries and the localized presence of late-stage albite on them, together with the absence of a preferred orientation of the late-stage albitic overgrowths on the plagioclase, demonstrates that these indentations are not a consequence of dissolution-reprecipitation in response to an applied stress but are most likely a consequence of irregular, late-stage growth of grains accumulated on the magma chamber floor. The scale bar is 1mm long. (b) a troctolitic cumulate from Lower Zone. Plagioclase is dark teal, with dark relatively albitic rims. Olivine is grey and augite is bright blue. Low-Ca pyroxene (inverted pigeonite) is a mottled grey. The cores of the plagioclase grains formed close to the magma-mush interface while the constant composition relatively sodic rims formed within the mush. The scale bar is 2 mm long.

1
2
3
4
5
6
7
8
9
10
11
12
13
14
15
16
17
18
19
20
21
22
23
24
25
26
27
28
29
30
31
32
33
34
35
36
37
38
39
40
41
42
43
44
45
46
47
48
49
50
51
52
53
54
55
56
57
58
59
60

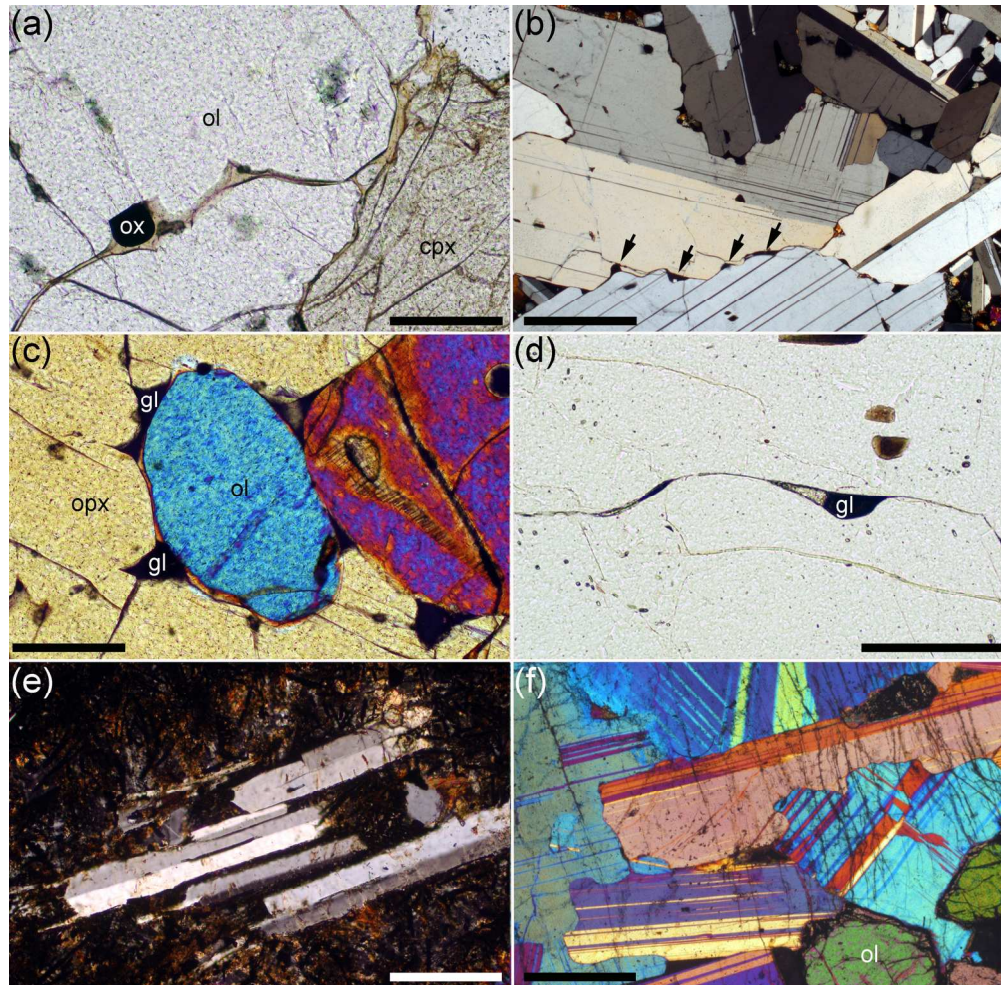
152x257mm (600 x 600 DPI)

For Review Only



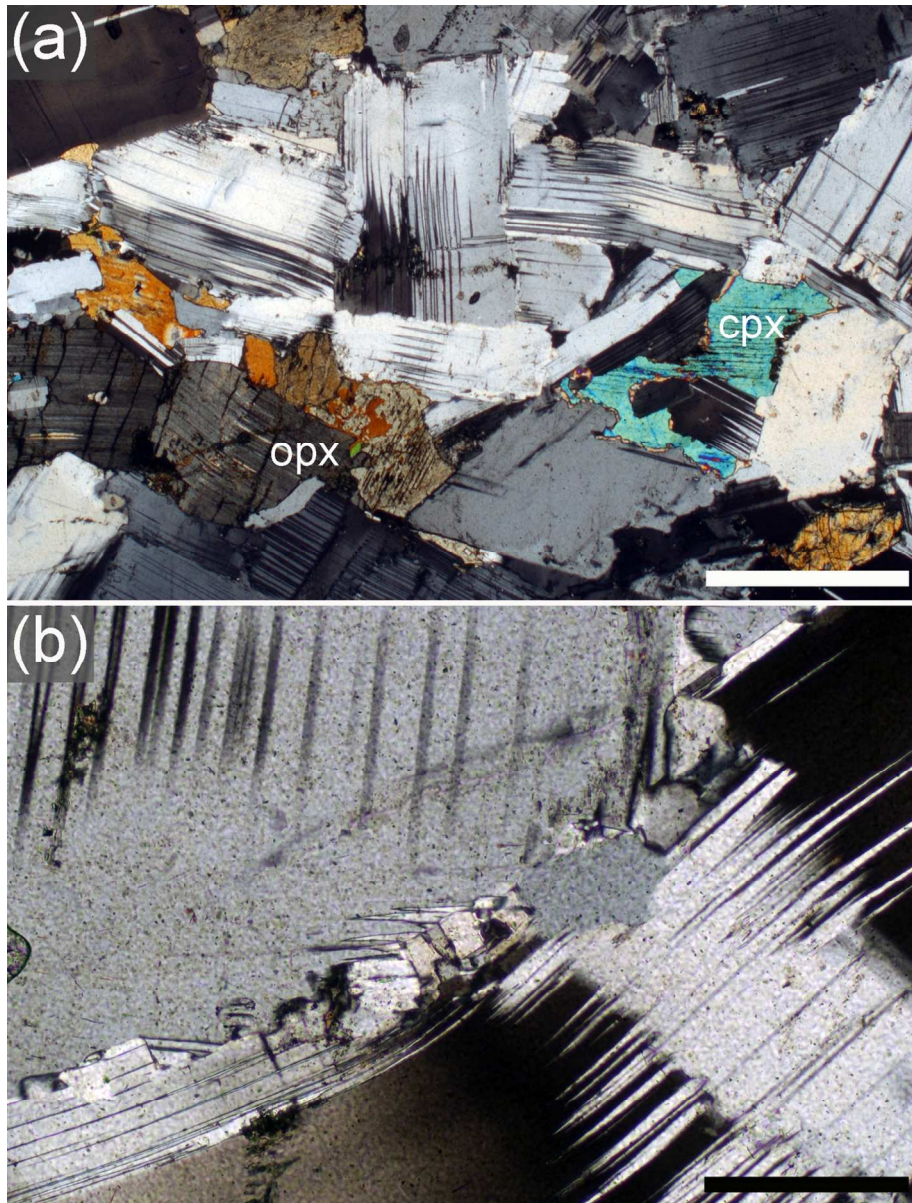
(a) Glass-rich portion of the upper crust of the Kilauea Iki lava lake, quenched during drilling. Plagioclase (labelled plag), augite (labelled cpx) and ilmenite (opaque) form a framework with interstitial brown glass (labelled glass). The junctions between adjacent grains are formed by the meeting of planar growth faces (examples are arrowed) with no evidence for minimization of interfacial energies. Plane polarized light. Scale bar is 1 mm long. (b) Plagioclase-rich glassy enclave from Brandur, Iceland, photographed with sensitive tint plate under crossed polars. The glass-filled pores have rounded cusped margins, with low, equilibrium values of the melt-plagioclase-plagioclase dihedral angle established at pore corners (examples are arrowed). Scale bar is 0.5 mm long. (c) Olivine-rich glassy enclave from Mauna Loa, Hawaii. The rounded olivine grains display dihedral angles close to textural equilibrium at pore corners. Plane polarized light. Scale bar is 0.5 mm long. (d) Troctolitic cumulate from the Eastern Layered Intrusion of the Rum Igneous Complex, Inner Hebrides. Three-grain junctions involving only plagioclase are close to textural equilibrium, with a well-developed granular microstructure in plagioclase-only regions. Note the absence of any evidence of planar plagioclase growth faces, in contrast to Fig. 1a. The olivine grain on the right has a low dihedral angle where it forms a three-grain junction with two plagioclase grains (arrowed), demonstrating an absence of textural equilibration of this poly-phase junction. Crossed polars. Scale bar is 0.5 mm long.

117x77mm (300 x 300 DPI)



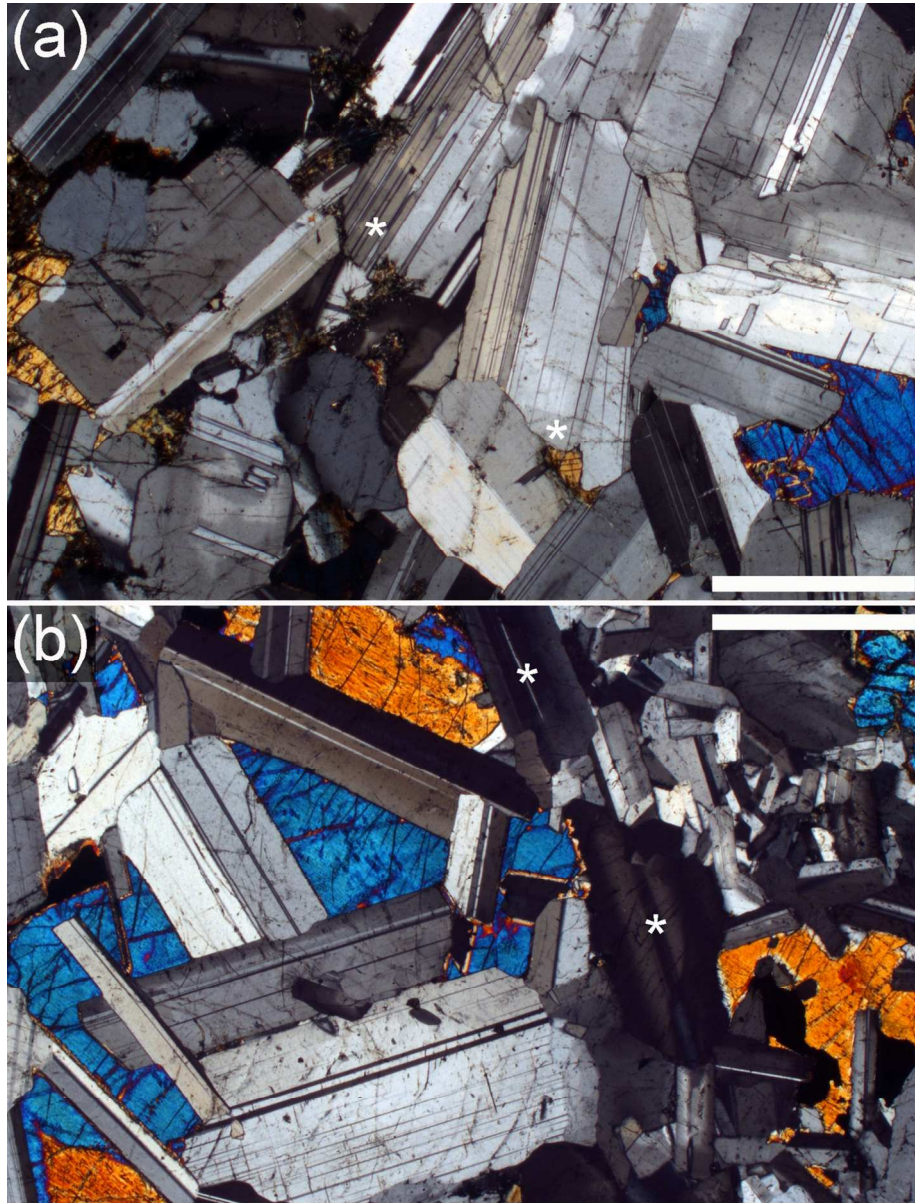
(a) glassy crystalline enclave from Mauna Loa, Hawaii, with an irregular glass film separating grains of olivine (ol) and augite (cpx). Note the small grain of spinel (labelled ox) sitting in the melt film, demonstrating its primary origin during solidification. Plane polarized light. Scale bar is 0.5 mm long. (b) Plagioclase-rich glassy enclave from Brandur, Iceland, showing lenses of glass (examples are arrowed) on irregular grain boundaries. Crossed polars. Scale bar is 1mm long. (c) glassy crystalline enclave from Mauna Loa, Hawaii, with irregular glass pockets (some of which are labelled gl) on boundaries between olivine and orthopyroxene (labelled opx). Note the low dihedral angles at pore corners, denoting approach to super-solidus textural equilibrium. Crossed polars. Scale bar is 0.5 mm long. (d) Plagioclase-rich enclave from Brandur, Iceland, showing a small pocket of glass on a plagioclase-plagioclase grain boundary, now partially infilled by clinopyroxene. Plane polarized light. Scale bar is 0.5 mm long. (e) The chilled margin of the Bracken Bay-Straiton Dyke, SW Scotland, showing a cluster of plagioclase phenocrysts set in a fine-grained groundmass. Note the alignment of the plagioclase and that they are joined along large areas of planar grain boundary parallel to the growth faces. Crossed polars. Scale bar is 0.5 mm long. (f) Gabbro from the Marginal Border Series of the Skaergaard Intrusion, East Greenland, showing highly irregular grain boundaries between adjacent plagioclase grains. Very few of these grain boundaries are parallel to growth faces of the plagioclase. Crossed polars with sensitive tint plate. Scale bar is 1 mm long.

176x173mm (300 x 300 DPI)



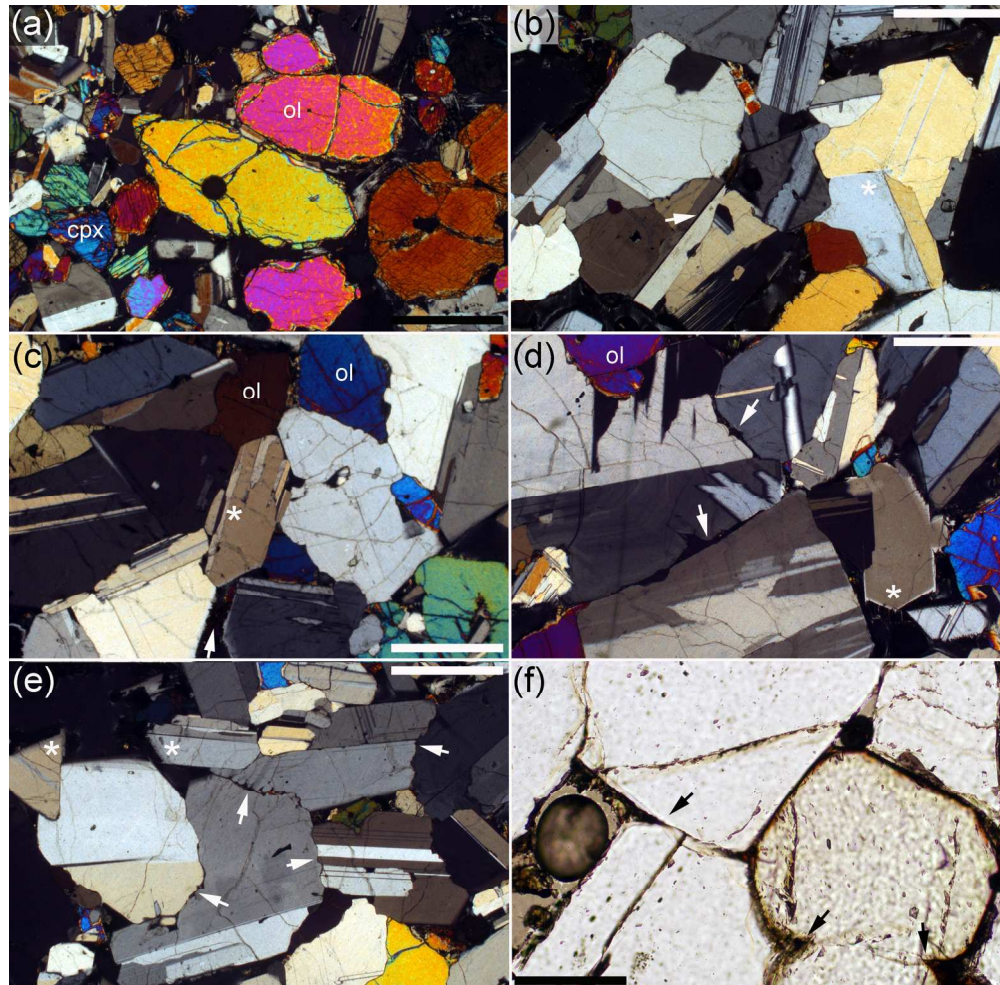
45 Cumulates from Middle Zone of the Rustenburg Layered Series of the Bushveld Complex, South Africa. (a)
46 Note the abundant tapering and curved deformation twins in the plagioclase, and the irregular grain
47 boundaries. Cumulus orthopyroxene grains are also bent although neighbouring interstitial clinopyroxene is
48 not strongly deformed. Crossed polars. Scale bar is 1 mm long. (b) Grain boundaries between strongly
49 deformed, original igneous, plagioclase grains are decorated with undeformed neoblasts that grew as a
50 result of dynamic recrystallization. Crossed polars. Scale bar is 0.5 mm long

51 117x154mm (300 x 300 DPI)



Sample 458220 from Lower Zone (LZa) of the Skaergaard Layered Series, in which plagioclase is cumulus and augite in interstitial. Note the small range in plagioclase grain sizes and the wide constant composition relatively albitic rims (examples are marked with an asterisk). This sample has only a very weak fabric. Crossed polars. Scale bar is 1 mm long. (a) Sample from the LZa equivalent in the Marginal Border Series. Note the wide range of grain sizes of the plagioclase and the abundant normal zoning (examples are marked with an asterisk). Crossed polars. Scale bar is 1 mm long.

117x154mm (300 x 300 DPI)



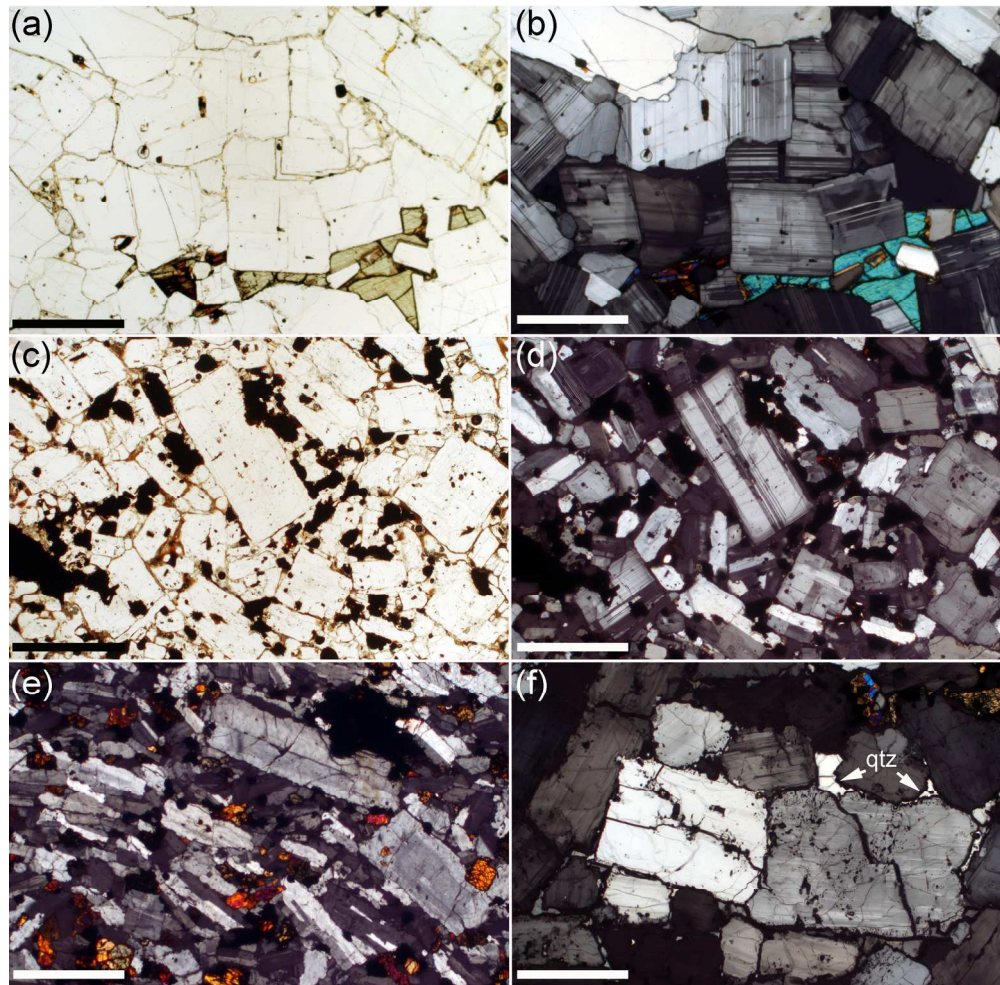
Troctolitic and gabbroic glass-bearing enclaves entrained in the 1950 andesite flow of the Kameni Islands, Santorini. (a) Clusters of euhedral to subhedral olivine and augite grains, joined by large areas of planar grain boundary consistent with a formation during synneusis. Crossed polars. Scale bar is 1 mm long. (b) Plagioclase grains in this enclave have low aspect ratios, commonly with complex twinning, and no evidence for dislocation creep (the yellow birefringence colour is due to the thickness of this thin section). The arrowed grain boundary is planar, melt-free and joins two plagioclase grains on their (010) faces: this is suggestive of sintering following synneusis. The grain marked with an asterisk is joined by similarly straight, (010) parallel grain boundaries to adjacent grains. Crossed polars. Scale bar is 1 mm long. (c) While many plagioclase grains have low aspect ratio, some are more elongate, with evidence of sintering following synneusis (grain marked with an asterisk). Note the planar growth faces where plagioclase is adjacent to large pockets of melt (example is marked by an arrow). Crossed polars. Scale bar is 1 mm long. (d) The grain marked with an asterisk has planar growth facets where it protrudes into a large melt-filled pocket (note the serrated, pale grey margins – these grew rapidly after entrainment). The two arrows show the location of wide melt-filled boundaries bounded by highly irregular plagioclase growth faces. Continued growth of these grains will result in the trapping of residual melt to form impingement lenses. Crossed polars. Scale bar is 1 mm long. (e) The two white arrows on the left denote wide melt films on developing grain boundaries between plagioclase grains, whereas those on the right show the location of highly irregular grain boundaries formed by impingement growth. Crossed polars. Scale bar is 1 mm long. (f) The rounded olivine grains have low dihedral angles where in contact (arrowed) denoting some approach to textural equilibrium at pore corners. There is rather less evidence of textural equilibration at plagioclase-plagioclase junctions, with some rounding caused by diffusion-limited late-stage growth during quenching

1
2
3
4
5
6
7
8
9
10
11
12
13
14
15
16
17
18
19
20
21
22
23
24
25
26
27
28
29
30
31
32
33
34
35
36
37
38
39
40
41
42
43
44
45
46
47
48
49
50
51
52
53
54
55
56
57
58
59
60

(an example on the left of the image is arrowed – note the clearly defined smooth inner surface of the overgrowth rim compared with the more irregular outer surface adjacent to the interstitial quenched glass; Holness et al., 2012b). Plane polarised light. Scale bar is 0.5 mm long.

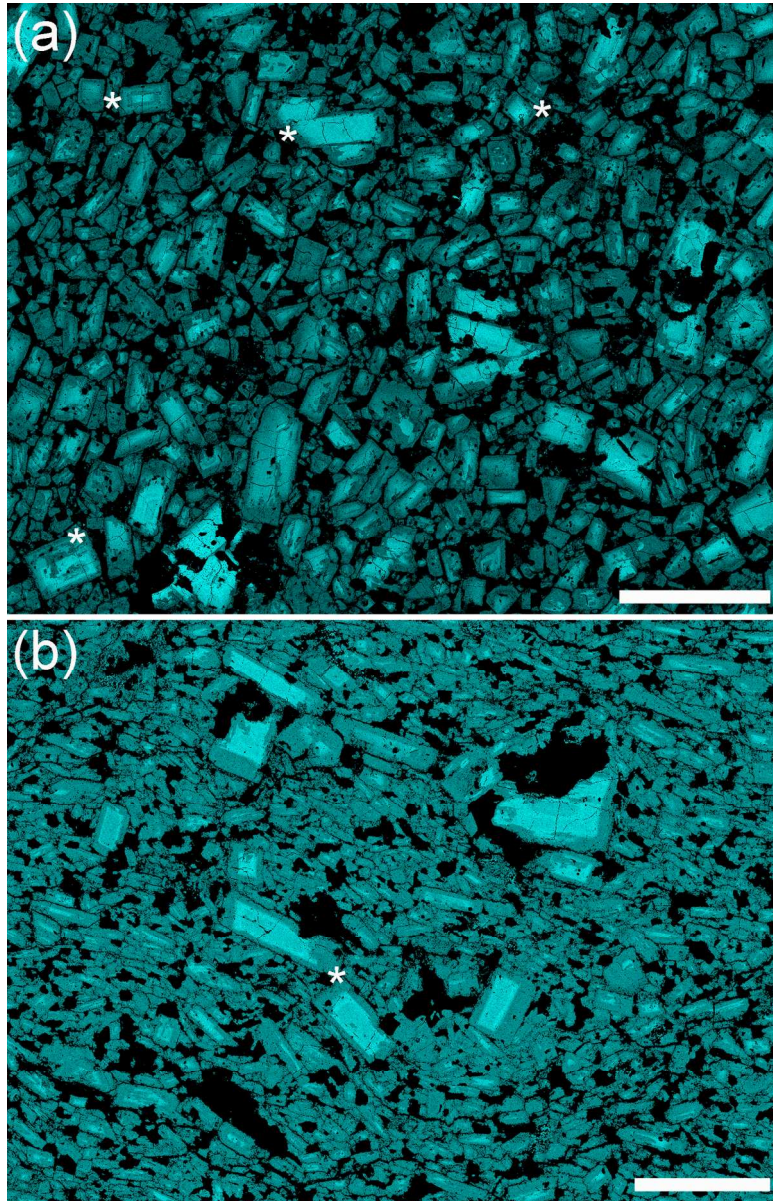
176x173mm (300 x 300 DPI)

For Review Only



Photomicrographs of the Rábida enclaves, Galápagos. (a) Plagioclase-rich enclave, with interstitial clinopyroxene and vesicular glass, photographed under plane polarised light. (b) shows the same area photographed under crossed polars. Note the absence of preferred orientation of the euhedral, low aspect ratio, plagioclase grains, their uniform grain size, and the frequency with which grain boundaries are formed by the juxtaposition of planar growth faces. Scale bar in both images is 1 mm long. (c) Plagioclase-rich enclave, with abundant small rounded grains of oxide and interstitial vesicular glass, photographed under plane polarised light. (d) shows the same area photographed under crossed polars. The range of grain sizes in this enclave is large, and the larger grains are commonly normally zoned. Note the evidence for complex zoning, with other grains apparently not zoned at all. The scale bar in both images is 1 mm long. (e) A strong preferred orientation of relatively elongate plagioclase. Note the scattering of small equant clinopyroxene grains. Crossed polars. Scale bar is 1 mm long. (f) Euhedral, equant plagioclase grains are separated by irregular but parallel-sided voids, with some transgranular fractures. The grain boundary voids are likely to have been created by decompaction caused by devolatilisation of interstitial melt during ascent. Note the interstitial quartz (labelled qtz; examples are arrowed), which is also separated from the adjacent plagioclase by parallel-sided voids. Crossed polars. Scale bar is 1 mm long

176x173mm (300 x 300 DPI)

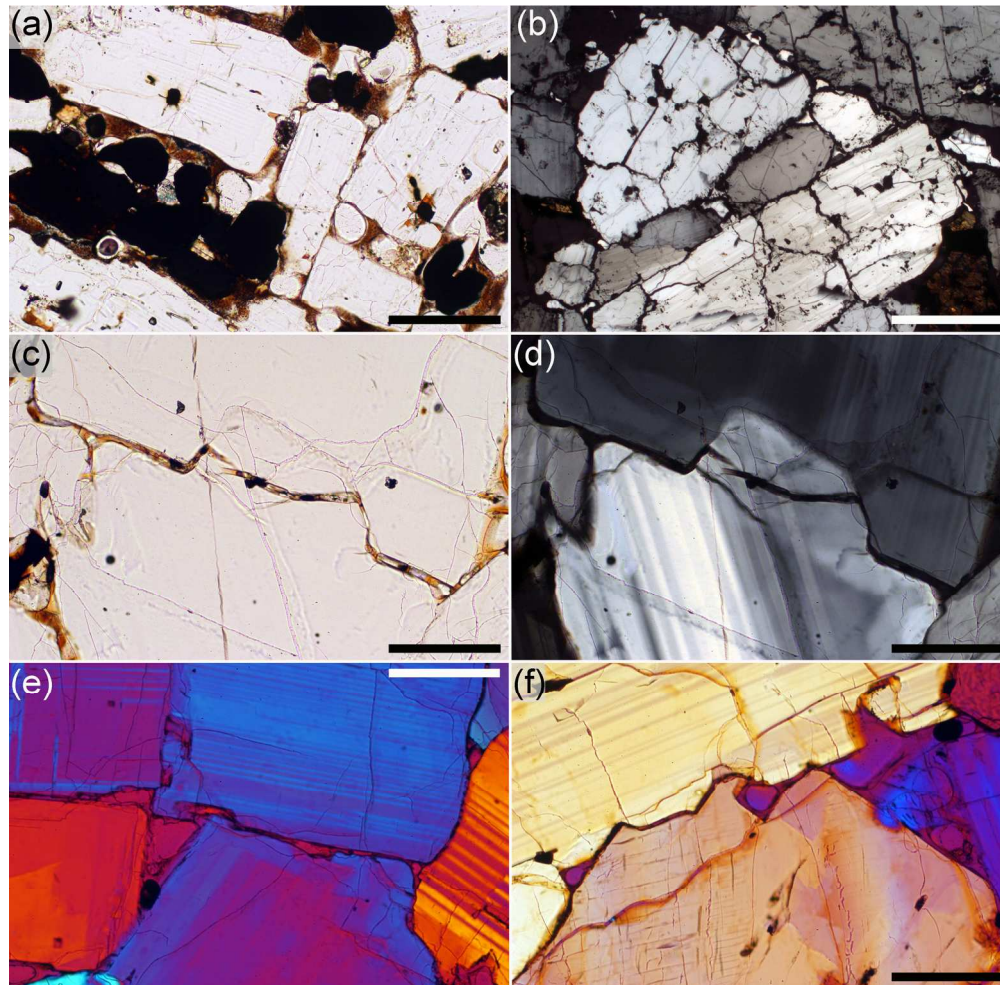


45 QEMSCAN images highlighting the Ca content of plagioclase in the Rábida enclaves, Galápagos. Bright
46 colours denote high Ca content and the darker teal more albitic compositions: phases other than plagioclase
47 are black in these images. (a) same enclave as depicted in Figures 7c and d. Note the presence of several
48 different zoning patterns, with particular examples of either normal, patchy or oscillatory zoning marked by
49 asterisks. It is not possible to reproduce this range of apparent zoning types by sectioning through a single
50 type. Scale bar is 2 mm long. (b) same enclave as depicted in Figure 7e. The two large plagioclase grains
51 either side of the asterisk are the two larger grains shown in Figure 7e. Note the strong preferred
52 orientation. The relatively larger grains in this field of view have strongly calcic cores, in contrast to the
53 majority of the smaller grains which have complex partially resorbed cores attesting to a different growth
54 history. Scale bar is 2 mm long.

55 138x214mm (300 x 300 DPI)

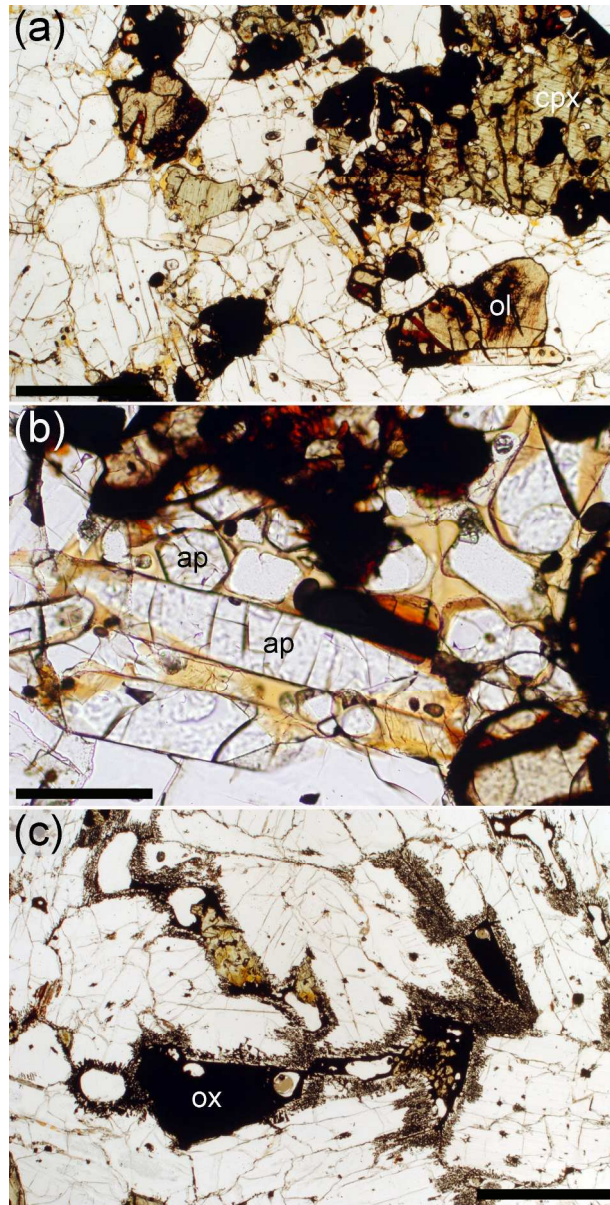
1
2
3
4
5
6
7
8
9
10
11
12
13
14
15
16
17
18
19
20
21
22
23
24
25
26
27
28
29
30
31
32
33
34
35
36
37
38
39
40
41
42
43
44
45
46
47
48
49
50
51
52
53
54
55
56
57
58
59
60

For Review Only



Photomicrographs of the Rábida enclaves, Galápagos. (a) Euhedral plagioclase and rounded grains of Fe-Ti oxides, set in highly vesicular interstitial glass. Plane polarised light. Scale bar is 0.5 mm long. (b) All grain boundaries in this enclave have been opened and are now either voids or locally contain some vesicular glass. Note the abundant interstitial quartz. Crossed polars. Scale bar is 1 mm long. (c) A grain boundary containing vesicular glass separates two plagioclase grains, photographed under plane polarised light. The same area is photographed under crossed polars in (d), in which it is apparent that the grain boundary has been opened by decompaction caused by devolatilisation during ascent, as the newly opened fracture also cuts one of the plagioclase grains. Scale bar in both images is 0.5 mm long. (e) Interstitial pockets of vesicular glass are bounded by either planar plagioclase growth faces (with localised limited approach to texturally equilibrated dihedral angles) or form impingement lenses along grain boundaries. Crossed polars with a sensitive tint plate. Scale bar is 0.5 mm long. (f) Irregular grain boundary between two plagioclase grains, containing vesicular glass. Crossed polars with a sensitive tint plate. Scale bar is 0.5 mm long.

176x173mm (300 x 300 DPI)



- Photomicrographs of the Rábida enclaves, Galápagos. (a) Enclave containing primocrysts of plagioclase, clinopyroxene, Fe-Ti oxides, with abundant apatite. The central part of this image is magnified in (b) Plane polarized light. Scale bar is 1 mm long. (b) Primocrysts of apatite ((labelled ap) are concentrated in or adjacent to pockets of glass, demonstrating that they crystallised relatively late. Plane polarized light. Scale bar is 0.5 mm long. (c) Plagioclase adjacent to pockets of (oxidized) glass or minerals that arrive relatively late on the liquidus has developed a sieve texture consistent with partial melting of the most evolved (and hence with the lowest temperature of crystallization) regions of the enclave during entrainment and ascent in a relatively hot magma. Plane polarized light. Scale bar is 1 mm long.!! +

176x347mm (300 x 300 DPI)